Reduced-RF-Chain Aided Soft-Decision Multi-Set Steered Space-Time Shift-Keying for Millimeter-Wave Communications

Ibrahim A. Hemadeh, *Student Member, IEEE,* Panagiotis Botsinis, *Member, IEEE,* Mohammed El-Hajjar, *Senior Member, IEEE,* SeungHwan Won[*], *Senior Member, IEEE,* and Lajos Hanzo, *Fellow, IEEE*

School of Electronics and Computer Science, University of Southampton, Southampton SO17 1BJ, U.K., (*) University of Southampton Malaysia Campus (USMC), Nusajaya, Johor, Malaysia

Tel: +44-23-8059 3125, Fax: +44-23-8059 4508

E-mail:{ih1g11, p.botsinis, meh, sw6f12, lh}@ecs.soton.ac.uk, http://www-mobile.ecs.soton.ac.uk

Abstract—**Soft-decision-aided Multi-Set Steered Space-Time Shift Keying (MS-SSTSK) intrinsically amalgamated with channel coding is proposed in order to attain near capacity-performance. Multi-Set Space-Time Shift Keying (MS-STSK) is a Multiple-input Multiple-output (MIMO) scheme, which combines the concepts of Spatial Modulation (SM) and STSK for the sake of achieving high data rates and enhanced system integrity. Furthermore, MS-STSK is combined with Orthogonal Frequency-Division Multiplexing (OFDM) as well as Single-Carrier Frequency Domain Equalization (SC-FDE) and additionally enhanced by analogue beamforming in order to support communications at Millimeter Wave (mmWave) frequencies. Given that OFDM-based SM systems cannot directly benefit from the reduced number of RF chains of SM due to the spreading effects of the Fast-Fourier Transform (FFT) and they suffer from a high Peak-to-Average Power Ratio (PAPR), we opt for employing the SC-based arrangement. The soft-decision-aided detector of the SC-based MS-STSK is combined with Recursive Systematic Convolutional (RSC) encoding and iterative detection at the receiver side in order to achieve excellent performance within 1.1 dB and 1.4 dB from the capacity limit for the soft-decision MS-STSK system and within 1.1 dB from the capacity limit for the SC-FDE-aided soft-decision MS-STSK. We also use EXtrinsic Information Transfer (EXIT) charts for analyzing our systems and evaluate their achievable rates.**

Index Terms—**Millimeter-Wave Communications, MIMO, Space-Time Shift Keying, Spatial Modulation, Multi-Set Space-Time Shift Keying, Single-Carrier, OFDM, EXIT charts.**

NOMENCLATURE

ABF	Analogue Beamforming
AC	Antenna Combination
AWGN	Additive White Gaussian Noise
BER	Bit Error Rate
BLAST	Bell-Labs Layered Space-Time
BPC	Bits Per Codeword
CC	Convolutional Coding
CSI	Channel State Information
DAC	Distinct AC
EXIT	EXtrinsic Information Transfer
FDE	Frequency Domain Equalization
LDC	Linear Dispersion Coding
LLR	Log Likelihood Ratio
Log-MAP	Logarithmic Maximum *a posteriori*
MIMO	Multiple-Input Multiple-Output
ML	Maximum Likelihood
MMSE	Minimum Mean Square Error
mmWave	Millimeter-Wave
MS-STSK	Multi-Set Space-Time Shift Keying
MS-SSTSK	Multi-Set Steered Space-Time Shift Keying
OFDM	Orthogonal Frequency-Division Multiplexing
RA	Receive Antenna
RAA	Receive Antenna Array
SAC	Shared AC
SISO	Soft-Input Soft-Output
RSC	Recursive Systematic Convolutional
ST	Space-Time
STSK	Space-Time Shift Keying
SM	Spatial Modulation
SNR	Signal-to-Noise Ratio
SC	Single-Carrier
TA	Transmit Antenna
TAA	Transmit Antenna Array
ZF	Zero-Forcing

I. INTRODUCTION

The community's interest in the millimetre wave (mmWave) frequency band has significantly increased during the last few years due to its substantial bandwidth reserves [1], [2], which is capable of mitigating the ever-growing wireless capacity demand [3]. Regretfully, mmWaves suffer however from a high path-loss and shadowing losses due to their short wavelengths, spanning from say $1\,mm$ to $10mm$ [4]. As a benefit however, a high number of $\lambda/2$-spaced Antenna Elements (AEs) can be integrated into a relatively compact area at both the transmitter and receiver sides for the sake of involving beamforming to compensate for the path-loss. Hence, with the aid of utilizing advanced Multiple-input Multiple-output (MIMO) techniques this compact structure is a substantial advantage [5].

Enhanced MIMO techniques designed for the mmWave band constitute key enabling components of wireless systems [6]. They have been extensively studied over the past two decades [7] in order to benefit from their advantageous diversity, multiplexing and beamforming gains. Furthermore, multiple techniques have been specifically designed for mmWave frequencies [6], [8], [9] to further benefit from the wide band-

|	
N_{RF}^t	Number of transmit RF chains
N_{RF}^r	Number of receive RF chains
N_s	Number of TAAs
N_{AA}^t	Number of AEs per TAA
N_{AA}^r	Number of AEs per RAA
θ_c	Phase shift rotation
$\mathcal{O}(.)$	Complexity order
M_Q	Number of dispersion matrices, where $q = 1, \ldots, M_Q$
M_c	Constellation size, where $l = 1, \ldots, M_c$
N_c	Number of AC combinations
T	Number of STSK time slots
M	Number of STSK spaces
B_1	Number of bits fed into the STSK encoder
B_2	Number of bits transmitted over the AC index
B	Number of the MS-STSK encoded bits
$\tilde{\mathbf{X}}$	MS-STSK codeword
$\tilde{A}_{q,c}$	MS-STSK dispersion matrix
s_l	QAM/PSK symbol
$\bar{\mathbf{Y}}$	Vectorized received singal
$\bar{\mathbf{H}}$	Vectorized equivalent channel
$\mathbf{H_c}$	Activated combination effective channel
$\mathbf{h}_{c,q}$	The q-th column of the c-th effective channel $\mathbf{H_c}$
$\mathcal{X}$	Vectorized MS-STSK dispersion matrices
$\mathcal{I}$	AC activation matrix
$\mathbf{I_C}$	Identity matrix at the c-th position in $\mathcal{I}$
$\mathbf{K}$	QAM/PSK symbol activation vector
$\triangle\theta_c$	Phase-shift difference between two ACs
$\hat{s}_l$	The estimate of the l-th transmitted symbol
$L_e(b_k),$	The extrinsic LLR of $b_k \in \mathbf{b}$
$\mathbf{b}$	Transmitted set of B bits
$R_{MS-STSK}$	MS-STSK system achievable throughput
$R_{MS-STSK}^{(SC-FDE)}$	The achievable throughput of the SC-based MS-STSK system
$R_{MS-STSK}^{(OFDM)}$	The achievable throughput of the OFDM-based MS-STSK system

Table I
LIST OF SYMBOLS.
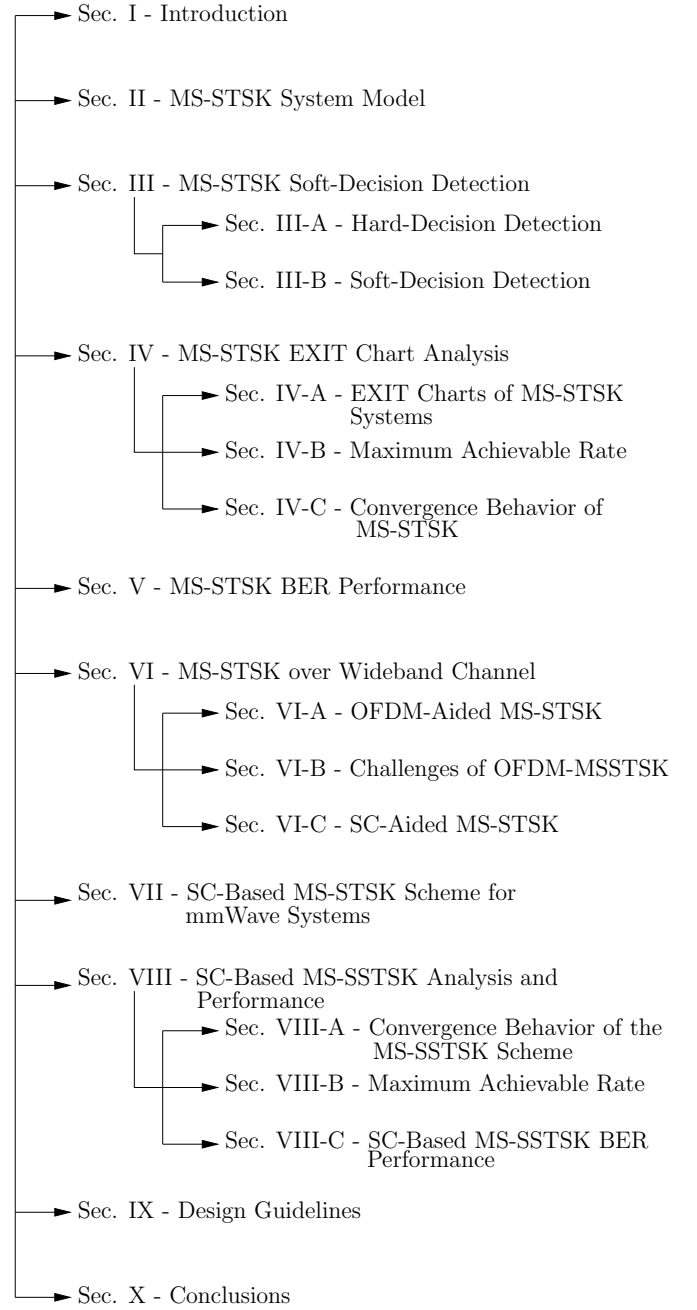
Figure 1. Treatise Structure.

width available.

Spatial Modulation (SM) was proposed in [10], [11], where extra information is implicitly conveyed over the activated antenna index used for transmitting a single classic QAM/PSK symbol. The key advantage of SM lies in its ability to achieve several MIMO benefits with the aid of a low-complexity single-radio frequency (RF) chain based architecture at the transmitter [12]–[16]. Combined with Linear Dispersion Codes (LDC), the encoding philosophy of SM was conceived in [17], [18] by activating one out of several dispersion matrices in order to achieve extra diversity gain by the Space-Time Shift Keying (STSK) scheme. In STSK, information is conveyed by transmitting a codeword consisting of a single dispersion

matrix and a single symbol over multiple antennas. Both techniques were then extended to the generalized SM (G-SM) [19] and the generalized STSK (GSTSK) regime [20], where different symbols are transmitted over multiple activated antennas in the G-SM and multiple dispersion matrices are activated by different symbols in the GSTSK arrangement. Recently, the concept of Multi-Set Space-Time Shift Keying (MS-STSK) was proposed in [21], where a carefully selected fraction of the antennas out of a larger number of antennas are activated to transmit a single STSK codeword associated with a phase-shift. This scheme was shown to outperform the ordinary STSK scheme, with the additional advantage of avoiding the inter-antenna interference issues imposed both by G-SM and GSTSK. The MS-STSK scheme is capable of striking a flexible trade-off between the attainable throughput and the achievable diversity gain.

Due to the high available bandwidth and the associated high sampling rates needed at the receiver, the mmWave channel is modeled as a dispersive wideband channel [22]–[24]. Naturally, its Channel Impulse Response (CIR) can be characterized by the classic Tapped Delayed Line (TDL) model [25]. To operate over mmWaves, wireless systems typically employ wideband techniques [6], [8], such as Orthogonal Frequency Division Multiplexing (OFDM) [26] and Single-Carrier Division Multiplexing (SC-DM) [27]. Furthermore, due to the short wavelengths of mmWaves, a high number of antennas can be integrated in a relatively compact area [1], which enables the system to employ large-scale antenna arrays (AAs) for the sake of achieving high beamforming gains [9], [28], [29]. This gain is essential at mmWaves and it is considered as a key prerequisite of operating over this band, exhibiting a high path-loss and a sparse CIR [30]. For example, a hybrid beamforming architecture was intrinsically amalgamated with MIMO-OFDM in [31] in order to operate over mmWaves. Similarly, Hemadeh *et al.* proposed in [8] a space-time solution combined with Analogue Beamforming (ABF) to overcome the high path losses of mmWaves.

OFDM-based SM was proposed in [32], where the system can still outperform the Vertical-Bell Laboratories Layered Space-Time (V-BLAST), albeit at the cost of surrendering the main advantage of SM of having a single-RF chain. In order to maintain a single-RF chain aided structure in OFDM-based SM schemes, the index of the activated antenna can be implicitly conveyed per OFDM block, rather than per sub-carrier. Moreover, the OFDM signals suffer from a high Peak-to-Average Power Ratio (PAPR), which would increase the power consumption of the power amplifier at mmWaves [33]. Hence, SC-based SM systems may be considered to constitute a better alternative, where the benefit of having a reduced number of RF-chains can be maintained at a low PAPR and a complexity comparable to that of OFDM [34].

High data-rate communication is required for satisfying the increasing thirst sophisticated wireless receivers [3], [7]. However, reliable transceiver designs and appropriate coding techniques are required for exploiting the mmWave band.

According to Shannon [35], introducing redundancy into the transmitted signal by relying on a *channel encoding operation* is capable of providing communication systems with reliable information transmission. Accordingly, diverse channel coding techniques were proposed, such as Hamming coding in 1950 [36], Convolutional Codes (CC) advocated by Elias in 1955 [37], turbo coding conceived by Berrou *et al.* in 1993 [38] as well as other coding techniques [39]. Various decoding algorithms were proposed in the literature for CC, such as the high complexity Maximum A Posteriori (MAP) algorithm [40], which constitutes the minimum Bit Error Rate (BER) solutions for CC codes. In the ensuing era, the concept of turbo codes has evolved to a wide range of iterative techniques associated with both parallel concatenated and serially concatenated architectures [38], [41], [42]. Hence, communication systems are capable of achieving near-capacity performance by relying on soft-decision detection, where the detector is capable of iteratively exchanging extrinsic information with a dedicated channel encoder [43], [44]. This system architecture can be studied and analysed using the powerful tool of EXtrinsic Information Transfer (EXIT) charts [42], [43], which can be also used for investigating the convergence of the iterative system and for evaluating its achievable rate.

In the context of STSK, several STSK soft-decision aided solutions were conceived by Kadir *et al.* in [45], [46]. In the context of SC systems, Pancaldi *et al.* proposed a soft-decision-aided SC system based on the Frequency Division Equalisation (FDE) technique in 2008 for Long Term Evolution (LTE) [47]. Then, Sugiura *et al.* [14] introduced a soft-decision aided detector for SC-SM, when SM was capable of transmitting efficiently over dispersive channels, while maintaining its single RF-chain fundamental advantage. In [14], a three-stage concatenated system was proposed for SC-SM based on the Minimum Mean-Squared Error (MMSE) FDE for attaining near-capacity performance. To expound a little further, this system considered a pair of Recursive Systematic Convolutional (RSC) codes and Unitary-Rate Convolutional (URC) codes amalgamated with an MMSE-based FDE detector, where extrinsic information was iteratively exchanged between these three components until no further enhancement in the output mutual information was detected.

Given that the MS-STSK scheme may be considered to be a branch of the MIMO-SM family tree, where the activated antenna combination index is conveyed implicitly along with the STSK codeword, employing wideband techniques such as the OFDM-based and SC-based arrangements is essential to operate over the mmWaves. The novel contributions of this paper are illustrated in Figure 2 and can be summarized as follows:

1) We propose the soft-decision aided decoder for MS-STSK of Figure 2 and then we propose a two-stage serially concatenated soft-decision based detector for the MS-STSK system intrinsically amalgamated with the antenna configuration techniques proposed in [21]. This system consists of a pair of inner and outer decoders, which iteratively exchange their intrinsic information for the sake of achieving near capacity performance.

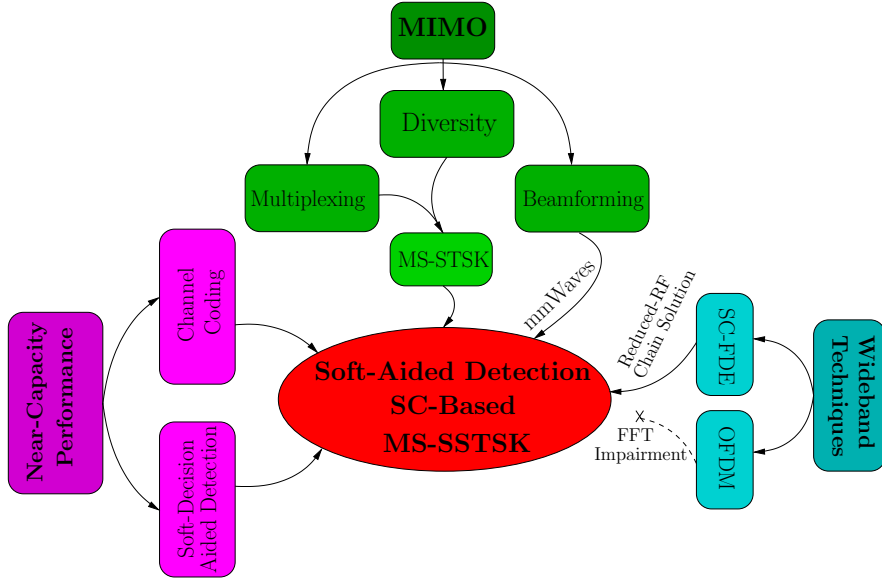2) We intrinsically amalgamate the MS-STSK concept both

Figure 2. The proposed soft-decision aided and SC-based MS-SSTK scheme is an amalgam of a sophisticated MIMO technique represented by the MS-STSK technique, a wideband technique based on SC-FDE and analogue beamforming. We optted for SC-based solution rather than for OFDM to avoid the FFT-induced impairments of the latter.

with OFDM and SC Frequency Domain Equalization (SC-FDE) associated with the proposed soft-decision detector for communication over wideband channels, as depicted in Figure 2. OFDM systems suffer from DFT and IDFT mismatch, when employing a reduced number of RF chains, while SC-based systems compensate the dispersion-induced performance degradation with the aid of channel equalization, despite using a reduced RF chains based deployment. Hence, OFDM-MSSTSK systems rely on enhanced signal processing techniques that aim for increasing both the attainable system throughput and the integrity. By contrast, SC-based MS-STSK systems additionally benefit from the MS-STSK scheme's reduced RF chain based solution.

3) Motivated by the advantages of the SC-based system over OFDM-based systems quantified in terms of the reduced number of RF chains and reduced PAPR, the soft-decision-aided SC-based MS Steered STSK (MS-SSTSK) system is recommended for mmWave channels operating with the aid of ABF achieved by a pair of phase-shifters and a single power amplifier, as shown in Figure 2. After applying FDE, the equalized signal is fed into the proposed iterative soft-decision decoder in order achieve a near-capacity performance.

4) We invoke the powerful tool of EXIT charts for analysing the convergence behavior of the proposed system and evaluate its achievable rate.

In the remainder of the paper, we present the MS-STSK system model in Section II and then introduce our soft-decision-aided detector in Section III. The proposed system is then evaluated in Section IV with the aid of EXIT charts. The BER performance of the soft-decision-based MS-STSK system is presented in Section V. In Section VI, we introduce both the OFDM-based and the SC-based MS-STSK systems

then the SC-based system is employed for mmWaves in Section VII. The SC-based system operating over mmWaves is evaluated using EXIT charts in Section VIII and we provide the corresponding Monte-Carlo simulation results in Section VIII-C. Next, in Section IX we present our design guidelines. Finally, we conclude in Section X.

Notations: Bold upper case letters represent matrices; $\lfloor . \rfloor$ denotes the operation of flooring a real number to the nearest smallest following integer, while $\lfloor . \rceil$ denotes the rounding operation of a real number to the nearest integer; $mod(.)$ indicates the modulus operation; $\begin{pmatrix} n \\ r \end{pmatrix}$ denotes the combinations without repetition of n objects taken r at a time; $(.)^T$ represents the transpose operation and $(.)^H$ represents the Hermitian transpose operation; $\mathbb{C}^{a \times b}$ indicates a matrix of complex numbers having the size $a \times b$; $\|.\|$ denotes the Frobenius norm and $|.|$ indicates the modulus of a complex number.

II. MS-STSK SYSTEM MODEL

In this section, we briefly describe the encoding procedure and the received signal model of the MS-STSK system [21]. Consider the MS-STSK transmitter shown in Figure 3 having M RF chains used for activating a specific combination out of the available N_t Transmit Antennas (TAs), with $M \leq N_t$, to transmit an $(M \times T)$-element STSK codeword over T time slots. In the MS-STSK encoder, the input bits are encoded over two separate stages, namely the STSK codeword generation and the Antenna Combination (AC) selection. The encoder uses the first $B_1 = \log_2(M_c M_Q)$ bits to generate an $(M \times T)$-element STSK codeword $\bar{\mathbf{X}} = A_q s_l$ over T time slots by spreading an M_c-sized QAM/PSK constellation symbol s_l over a single space-time dispersion matrix in the set $\{A_q\}_{q=1}^{M_Q}$, where M_Q is the total number of dispersion matrices and A_q satisfies the power constraint of $\text{tr}(A_q^H A_q) = T$ [17],

[18]. Next, in a similar fashion to SM, the encoder uses the following $B_2 = \log_2(N_c)$ bits in order to activate a single AC of the available TAs in the set $\{AC_c\}_{c=1}^{N_c}$, while other TAs remain silent, where N_c is the total number of ACs. In the context of MS-STSK, an AC is defined as a set of M AEs which once activated can implicitly transmit the predefined index associated with the $(M \times T)$-element STSK codeword. Furthermore, the MS-STSK encoder has an integrated space-time mapper that maps the serial output of the STSK encoder to its appropriate space and time indices. Finally, the MS-STSK codeword $\tilde{\mathbf{X}} = \tilde{A}_{q,c}s_l$ is transmitted from the M activated TAs, where $\tilde{A}_{q,c} \in \mathbb{C}^{N_t \times T}$ is the c-th equivalent dispersion matrix of MS-STSK. The achievable throughput in bits per MS-STSK codeword (bpc) of the system can be expressed as:

$$R_{MS-STSK} = \log_2\left(M_Q M_c N_c\right)\ (bpc). \tag{1}$$

In [21], a pair of AE allocation approaches were proposed for forming a single AC, namely either by using distinct AEs in each AC or by sharing one or more AEs in multiple ACs. For example, in order to implicitly transmit $B_2 = 2$ bits over the activated AC, $N_c = 2^{B_2} = 4$ ACs are required and the set of ACs having distinct AEs can be viewed as

$$\tilde{\mathbf{X}} = \begin{bmatrix} \tilde{\mathbf{x}}_1 \\ \tilde{\mathbf{x}}_2 \\ 0 \\ 0 \\ 0 \\ 0 \\ 0 \\ 0 \end{bmatrix}, \begin{bmatrix} 0 \\ 0 \\ \tilde{\mathbf{x}}_1 \\ \tilde{\mathbf{x}}_2 \\ 0 \\ 0 \\ 0 \\ 0 \end{bmatrix}, \begin{bmatrix} 0 \\ 0 \\ 0 \\ 0 \\ \tilde{\mathbf{x}}_1 \\ \tilde{\mathbf{x}}_2 \\ 0 \\ 0 \end{bmatrix} or \begin{bmatrix} 0 \\ 0 \\ 0 \\ 0 \\ 0 \\ 0 \\ \tilde{\mathbf{x}}_1 \\ \tilde{\mathbf{x}}_2 \end{bmatrix}, \tag{2}$$

where $\tilde{\mathbf{x}}_m \in \mathbb{C}^{1 \times T}$ represents the m-th activated row of $\tilde{\mathbf{X}}$, while the set of ACs sharing one or more AEs can be viewed as

$$\tilde{\mathbf{X}} = \begin{bmatrix} \tilde{\mathbf{x}}_1 \\ \tilde{\mathbf{x}}_2 \\ 0 \\ 0 \end{bmatrix}, \begin{bmatrix} \tilde{\mathbf{x}}_1 \\ 0 \\ \tilde{\mathbf{x}}_2 \\ 0 \end{bmatrix}, \begin{bmatrix} \tilde{\mathbf{x}}_1 \\ 0 \\ 0 \\ \tilde{\mathbf{x}}_2 \end{bmatrix} or \begin{bmatrix} 0 \\ \tilde{\mathbf{x}}_1 \\ \tilde{\mathbf{x}}_2 \\ 0 \end{bmatrix}. \tag{3}$$

It is clearly shown in (2) that $\tilde{\mathbf{x}}_1$ and $\tilde{\mathbf{x}}_2$ of each AC are located at different rows, while in (3) they can be located at the same row in multiple AC, where $\tilde{\mathbf{x}}_1$ is located in the first row in the first, second and third AC. By using the Distinct Antenna Combination (DAC) allocation approach, the MS-STSK system requires a total of $N_t = N_c \times M$ AEs, where the total number of ACs is expressed as

$$N_c = \frac{N_t}{M}, \tag{4}$$

while using the Shared Antenna Combination (SAC) allocation approach requires a lower number of AEs, where the total number of ACs is defined by

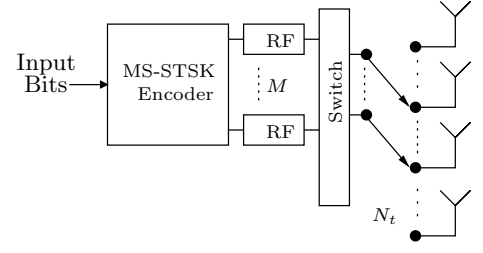$$N_c = \left\lfloor \binom{N_t}{M} \right\rfloor_{2^p}, \tag{5}$$

Figure 3. Block diagram an MS-STSK transmitter.

which is floored to the nearest base-2 integer. However, the reduced number of AEs in SAC comes at the cost of a degraded performance due to the AC correlation introduced by sharing one or more AEs in different ACs [21]. Fortunately, the performance of the MS-STSK system using SAC can be enhanced with the aid of applying a phase rotation θ_c to each STSK codeword of the c-th AC [21].

At the receiver side, which is equipped with N_r Receive Antennas (RAs), the $(N_r \times T)$-element received MS-STSK signal can be modelled as

$$\mathbf{Y} = \mathbf{H}\tilde{\mathbf{X}} + \mathbf{V}, \tag{6}$$

where $\mathbf{H} \in \mathbb{C}^{N_r \times N_t}$ denotes the channel matrix and $\mathbf{V} \in \mathbb{C}^{N_r \times T}$ represents the Additive White Gaussian Noise (AWGN) with zero mean and N_0 variance.

The vectorial stacking operation is applied to (6) in [21] in order to view the SM-equivalent model as

$$\bar{\mathbf{Y}} = \bar{\mathbf{H}}\mathcal{X}\mathcal{I}\mathbf{K}_{q,l} + \bar{\mathbf{V}}, \tag{7}$$

where the vectorized notations are given by [21]

$$\bar{\mathbf{Y}} = vec(\mathbf{Y}) \in \mathbb{C}^{N_r T \times 1}, \tag{8}$$

$$\bar{\mathbf{H}} = \mathbf{I}_T \otimes \mathbf{H} \in \mathbb{C}^{N_r T \times N_t T}, \tag{9}$$

$$\bar{\mathbf{V}} = vec(\mathbf{V}) \in \mathbb{C}^{N_r T \times 1}, \tag{10}$$

$$\mathcal{X} = [vec(\tilde{A}_{1,1}) \dots vec(\tilde{A}_{q,c}) \dots vec(\tilde{A}_{q,N_c})]$$
$$\in \mathbb{C}^{N_t T \times N_c M_Q}, \tag{11}$$

$$\mathcal{I} = [\mathbf{0}\dots \underset{\underset{c-th\,element}{\downarrow}}{\mathbf{I}_{M_Q}} \dots \mathbf{0}]^T \in \mathbb{C}^{N_c M_Q \times M_Q}, \tag{12}$$

$$\mathbf{K}_{q,l} = [\underbrace{0,\dots,0}_{q-1}, s_l, \underbrace{0,\dots,0}_{M_Q-q}]^T \in \mathbb{C}^{M_Q \times 1}, \tag{13}$$

where based on the c-th position of the $(M_Q \times M_Q)$-element identity matrix $\mathbf{I}_{M_Q}$ in $\mathcal{I}$, the c-th AC is activated and $\mathbf{K}_{q,l}$ represents the equivalent classic PSK/QAM symbol vector. Hence, Equation (7) can be represented as

$$
\bar{\mathbf{Y}} = \begin{bmatrix} \mathbf{H} & \cdots & \mathbf{0} \\ \vdots & \ddots & \vdots \\ \mathbf{0} & \cdots & \mathbf{H} \end{bmatrix}
$$

$$
\cdot \left[\cdots \begin{bmatrix} \hat{\mathbf{A}}_{1,c} & \cdots & \hat{\mathbf{A}}_{M_Q,c} \end{bmatrix} \cdots \right]
$$

$$
\cdot \begin{bmatrix} \mathbf{0} \\ \vdots \\ \mathbf{I}_{M_Q} \\ \vdots \\ \mathbf{0} \end{bmatrix}
$$

$$
\cdot \begin{bmatrix} 0 \\ \vdots \\ s_l \\ \vdots \\ 0 \end{bmatrix} + \bar{\mathbf{V}}, \tag{14}
$$

where $\hat{\mathbf{A}}_{q,c} = vec(\tilde{\mathbf{A}}_{q,c}) \in \mathbb{C}^{N_t T \times 1}$.

The system is referred in [21] to as MS-STSK(N_t, M, N_r, T, M_Q, M_cQAM/PSK) and it is associated with STSK(M, T, M_Q, M_c).

III. MS-STSK SOFT-DECISION DETECTION

In this section, we commence by reviewing a pair of conventional hard-decision detection techniques conceived for the MS-STSK scheme, namely the optimal Maximum Likelihood (ML) detector and the optimal Hard-Limiter (HL) aided ML detectors of [21]. Then, we introduce our proposed soft-decision-aided detection.

A. Hard-Decision Detection

Given the availability of Channel State Information (CSI) at the receiver, an optimal ML detector may be utilized for the sake of detecting the transmitted information using the vectorized system model shown in (7). The vector-by-vector ML detector may be formulated as [21]:

$$
< \hat{q}, \hat{l}, \hat{c} > = \arg\min_{q,l,c} \left\| \bar{\mathbf{Y}} - \bar{\mathbf{H}}\mathcal{X}\mathcal{I}_c\mathbf{K}_{q,l} \right\|^2, \tag{15}
$$

$$
= \arg\min_{q,l,c} \left\| \bar{\mathbf{Y}} - s_l \left(\bar{\mathbf{H}}_c\mathcal{X} \right)_q \right\|^2, \tag{16}
$$

where $\hat{q}$, $\hat{l}$ and $\hat{c}$ represent the estimates of the dispersion matrix index, the symbol constellation index and the AC index referred to as q, l and c, respectively, with $\left(\bar{\mathbf{H}}_c\mathcal{X} \right)_q$ denoting the q-th column vector of the c-th AC equivalent channel matrix.

The ML detector has a complexity order of $\mathcal{O}(M_Q M_c N_c)$, when its invokes full-search over all unique combinations of dispersion matrices, QAM/PSK symbols and ACs. For the sake of reducing the detection complexity order, another detector was proposed in [21] based on the HL-aided ML detector of [13], [48], which eliminates the M_c symbol constellation from the search-space, hence reducing the complexity order to $\mathcal{O}(M_Q N_c)$. In the HL-ML detector, the vector-by-vector Hermitian transpose of each column of the AC effective channel is defined by

$$
\mathbf{H_c} = \bar{\mathbf{H}}\mathcal{X}\mathcal{I}, \tag{17}
$$

where $\mathbf{H_c} = [\mathbf{h}_{c,1} \ldots \mathbf{h}_{c,M_Q}] \in \mathbb{C}^{N_r T \times M_Q}$ is constituted by M_Q column vectors, which is then applied to the vectorized received signal shown in (7) in the form of

$$
\hat{\mathbf{y}}_{c,q} = \frac{\mathbf{h}_{c,q}^H \bar{\mathbf{Y}}}{\|\mathbf{h}_{c,q}\|^2}, \tag{18}
$$

in order to acquire the estimate of the PSK/QAM symbol $\hat{s}_l$ at a given AC c and dispersion matrix q using direct amplitude and phase mapping for classic QAM constellations and phase mapping for PSK constellations. Then, a full search is applied over all unique combinations of dispersion matrices and ACs, which is formulated as

$$
< \hat{q}, \hat{c} > = \arg\min_{q,c} \left(|\hat{\mathbf{y}}_{c,q} - \hat{s}_l|^2 - |\hat{\mathbf{y}}_{c,q}|^2 \right) \|\mathbf{h}_{c,q}\|^2, \tag{19}
$$

in order to determine the estimates of both the dispersion matrix $\hat{q}$ and AC $\hat{c}$ at the symbol estimate $\hat{s}_l$.

B. Soft-Decision Detection

In this section, the previous hard-decision MS-STSK receiver is extended to support soft-decision detection. In soft-decision-aided detection, the soft-bit decision is determined with the aid of a Log Likelihood Ratio (LLR) defined by [43], [49]:

$$
L(b) = \log \frac{p(b=1)}{p(b=0)} \tag{20}
$$

$$
= \log \frac{p(b=1)}{1 - p(b=1)}, \tag{21}
$$

where the sign of $L(b)$ indicates the result of the associated hard decision and its magnitude $|L(b)|$ determines the hard decision's reliability. Hence, the probability of having a logical 1 or a logical 0 bit can be determined using the soft-value denoted by $L(b)$ as:

$$
p(b=1) = \frac{e^{L(b)}}{1 + e^{L(b)}}, \tag{22}
$$

or

$$
p(b=0) = \frac{1}{1 + e^{L(b)}}, \tag{23}
$$

respectively.

The block diagram of a two-stage concatenated MS-STSK system is shown in Figure 4, where the channel encoder of the transmitter encodes the input bits with the aid of a Recursive Systematic Convolutional (RSC) code to generate the bits stream c, which is then interleaved using the interleaver Π to produce the interleaved sequence u. The interleaver scrambles the bit sequence in order to disperse the bursty channel errors inflicted by deep fades, which lends beneficial time-diversity to the system [49]. The interleaved bits are then used for encoding the MS-STSK codewords using the encoder described in Section II. After mapping each codeword to its corresponding AC, the MS-STSK codewords are finally transmitted.

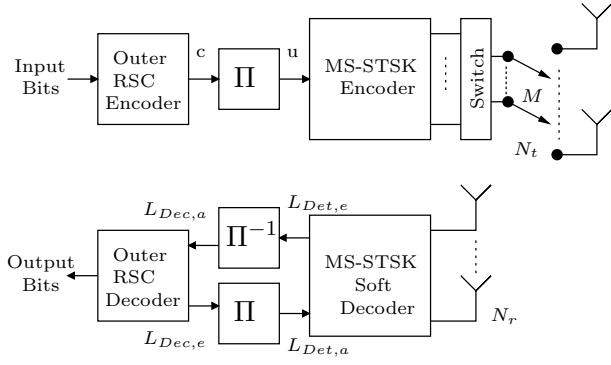At the receiver side of Figure 4, the MS-STSK Soft-Input

Figure 4. The transceiver architecture of the soft-decision-aided MS-STSK scheme.

Soft-Output (SISO) decoder iteratively exchanges its soft-information with the SISO RSC decoder. As shown in Figure 4, the received codewords are decoded using the two-stage soft-decision MS-STSK decoder. More specifically, the MS-STSK SISO decoder iteratively exchanges the extrinsic information $L_{Dec,e}$ with the RSC decoder. The SISO RSC decoder utilizes the Bahl-Cocke-Jelinek-Raviv (BCJR) algorithm [40], which converts the multiplication operations to additions by operating in the logarithmic domain and decodes the resultant soft values using the Logarithmic Maximum *a posteriori* (Log-MAP) algorithm [50], [51]. At each inner-outer decoder iteration, the MS-STSK detector's output LLRs $L_{Det,e}$ are deinterleaved by the deinterleaver Π^{-1} to produce the soft-bits $L_{Dec,a}$, which are fed into the RSC decoder as *a priori* LLRs. Then the RSC decoder generates the extrinsic LLRs $L_{Dec,e}$ using the Log-MAP algorithm, which are again interleaved using the interleaver Π and fed back into the MS-STSK detector as *a priori* LLRs $L_{Det,a}$. The input values of $L_{Det,a}$ are invoked for computing the improved values of $L_{Det,e}$ for the following iteration.

Here, rather than using the hard-decision detection Equations (16) and (19), we employ soft-decisions based on the classic Log-MAP algorithm [50], [51].

Following the probabilistic representation of the STSK decoder proposed in [18], the conditional probability of receiving the block signal $\bar{\mathbf{Y}}$ given that the $\mathbf{K}_{q,l}$-th symbol was transmitted over the c-th AC can be written as

$$
\begin{aligned}
p(\bar{\mathbf{Y}}|\mathbf{K}_{q,l,c}) &= \frac{1}{(\pi N_0)^{N_r T}} \exp\left(-\frac{\left\|\bar{\mathbf{Y}} - \bar{\mathbf{H}}\mathcal{X}\mathcal{I}_c\mathbf{K}_{q,l}\right\|^2}{N_0}\right) \quad (24) \\
&= \frac{1}{(\pi N_0)^{N_r T}} \exp\left(-\frac{\left\|\bar{\mathbf{Y}} - s_l\left(\bar{\mathbf{H}}_c\mathcal{X}\right)_q\right\|^2}{N_0}\right), (25)
\end{aligned}
$$

when using the estimate of the MS-STSK codeword in (16), where $\mathbf{K}_{q,l,c}$ represents the l-th symbol s_l dispersed over the ST domain by the q-th dispersion matrix and transmitted using the c-th AC denoted by $\left(\bar{\mathbf{H}}_c\mathcal{X}\right)_q$ in (16). The received signal $\bar{\mathbf{Y}}$ carries $B = B_1 + B_2 = \log_2\left(M_c M_Q\right) + \log\left(N_c\right) = \log_2(M_c M_Q N_c)$ coded bits $\mathbf{b} = [b_1, b_2, \ldots, b_B]$ and the extrinsic LLR of $b_k \in \mathbf{b}$, given that $k = 1, \ldots, B$, can be expressed by [39]

$$
L_e(b_k) = \log\left(\frac{\sum_{\mathbf{K}_{q,l,c} \in \mathbf{K}_1^k} \exp\left(\lambda_{q,l,c}\right)}{\sum_{\mathbf{K}_{q,l,c} \in \mathbf{K}_0^k} \exp\left(\lambda_{q,l,c}\right)}\right), \quad (26)
$$

where $\mathbf{K}_1^k$ and $\mathbf{K}_1^k$ denote the MS-STSK codeword sets satisfying the conditions of $\mathbf{K}_1^k \doteq \{\mathbf{K}_{q,l} \in \mathbf{K} : b_k = 1\}$ and $\mathbf{K}_0^k \doteq \{\mathbf{K}_{q,l} \in \mathbf{K} : b_k = 0\}$, respectively. Then, the intrinsic metric of the exponents $\lambda_{q,l,c}$ may be written as

$$
\lambda_{q,l,c} = -\frac{\left\|\bar{\mathbf{Y}} - s_l\left(\bar{\mathbf{H}}_c\mathcal{X}\right)_q\right\|^2}{N_0} + \sum_{j \neq k} b_j L_a(b_j), \quad (27)
$$

where $L_a(.)$ represents the *a priori* LLR shown in Figure 4 as the feedback from the outer RSC decoder to the MS-STSK decoder. However, in order to simplify the soft-decision aided detection of (26), we employ the Approximate Log-MAP (Approx-Log-MAP) algorithm of [43], [44] and the Maximum Log-MAP (Max-Log-MAP) algorithm of [39] as

$$
L_e(b_k) = \underset{\mathbf{K}_{q,l,c} \in \mathbf{K}_1^k}{\mathrm{jac}}\left(\lambda_{q,l,c}\right) - \underset{\mathbf{K}_{q,l,c} \in \mathbf{K}_0^k}{\mathrm{jac}}\left(\lambda_{q,l,c}\right), \quad (28)
$$

and

$$
L_e(b_k) = \max_{\mathbf{K}_{q,l,c} \in \mathbf{K}_1^k}\left(\lambda_{q,l,c}\right) - \max_{\mathbf{K}_{q,l,c} \in \mathbf{K}_0^k}\left(\lambda_{q,l,c}\right), \quad (29)
$$

respectively, where jac and max denote the Jacobian maximum and the maximum operations, respectively [49], [51].

IV. MS-STSK EXIT CHART ANALYSIS

In this section, we describe the EXIT chart [49] used for analyzing the convergence behavior of our soft-decision MS-STSK decoder associated with the DAC and the SAC approaches of Section II. The EXIT chart is a powerful tool conceived for visualizing the exchange of the extrinsic information between the concatenated decoders and for accurately predicting the convergence behavior of the iterative decoder based on the mutual information of the information exchanged [43], [52]. The EXIT characteristic of the RSC decoder shown in Figure 4 depicts the relationship between the *a priori* LLRs input into the RSC decoder $L_{Dec,a}$ and its corresponding output extrinsic LLRs $L_{Dec,e}$. Furthermore, the EXIT characteristic of the MS-STSK detector shown in Figure 4 describes the relationship between the *a priori* LLRs input to the MS-STSK detector $L_{Det,a}$ and the detector's output extrinsic LLRs $L_{Det,e}$. The EXIT curve of the MS-STSK detector depends also on the channel's output, represented by the received signal, which explains why the LLRs value varies for different SNR values. In order to visualize the information exchange of the decoders, the mutual information of the input and the output decoders is used, where $I_{Det,a}$ and $I_{Det,e}$ represents the mutual information of the input and the output LLRs of the MS-STSK detector, respectively, while $I_{Dec,a}$ and $I_{Dec,e}$ represents that of the RSC decoder always with respect to their respective values at the transmitter side.

A. EXIT Charts of MS-STSK Systems

We consider five MS-STSK systems having the same STSK($M = 2, T = 2, M_Q = 4, M_c = 4QAM$) encoder settings configured for transmitting 5, 6, 7, 8 and 9 bits over Rayleigh fading channels, where $B_1 = \log_2(4 \times 4) = 4$ bits are conveyed over the STSK codeword and $B_2 =$1, 2, 3, 4 and 5 bits are implicitly transmitted over the activated AC index. Hence, given that $B_2 = \log_2(N_c)$ bits are conveyed over the activated AC index, a total of 2, 4, 8, 16 and 32 ACs are required for carrying the additional bits, where $N_t = M \times N_c =$4, 8, 16, 32 and 64 AEs are needed, when utilizing the DAC approach denoted as MS-STSK(4, 2, 2, 2, 4, 4QAM), MS-STSK(8, 2, 2, 2, 4, 4QAM), MS-STSK(16, 2, 2, 2, 4, 4QAM), MS-STSK(32, 2, 2, 2, 4, 4QAM) and MS-STSK(64, 2, 2, 2, 4, 4QAM), respectively. By contrast, based on $N_c = \left\lfloor \binom{N_t}{M} \right\rfloor$, only $N_t =$3, 4, 5, 7 and 9 AEs are required by the SAC approach associated with an inter-combination phase-shift difference of $\triangle\theta = \theta_{c+1} - \theta_c = 12.5°$ based on [21], which are represented by the MS-STSK(3, 2, 2, 2, 4, 4QAM), MS-STSK(4, 2, 2, 2, 4, 4QAM), MS-STSK(5, 2, 2, 2, 4, 4QAM), MS-STSK(7, 2, 2, 2, 4, 4QAM) and MS-STSK(9, 2, 2, 2, 4, 4QAM) notations, respectively.

Figure 5 shows the EXIT charts of the DAC MS-STSK systems having $N_t = 4$ AEs and the SAC MS-STSK system having $N_t = 3$ AEs, respectively, recorded at SNR values ranging from -5.0 dB to 5.0 dB with a step size of 1.0 dB for each EXIT chart. The detector's input and output mutual information $I_{Det,a}$ and $I_{Det,e}$ are represented on the x-axis and y-axis, respectively. As shown in the figures, as the SNR value increases, the inner decoder's EXIT chart is shifted upwards. Similar trends are valid for the MS-STSK(8, 2, 2, 2, 4, 4QAM), MS-STSK(16, 2, 2, 2, 4, 4QAM), MS-STSK(32, 2, 2, 2, 4, 4QAM) and MS-STSK(64, 2, 2, 2, 4, 4QAM) systems associated with the DAC configuration, as well as for the MS-STSK(4, 2, 2, 2, 4, 4QAM), MS-STSK(5, 2, 2, 2, 4, 4QAM), MS-STSK(7, 2, 2, 2, 4, 4QAM) and MS-STSK(9, 2, 2, 2, 4, 4QAM) systems associated with the SAC configuration.

B. Maximum Achievable Rate

The EXIT charts of the above-mentioned systems can be used for determining the maximum achievable rate of the system [53], where the area $\mathcal{A}(E_s/N_0)$ under the EXIT curve $\mathcal{E}(E_s/N_0)$ of the inner code at a given SNR value E_s/N_0 can be used for determining the achievable rate of the system as $(R_{MS-STSK} \times \mathcal{A}(E_s/N_0))$ bits per second per Hertz (bps/Hz), where $\mathcal{A}(E_s/N_0)$ is given by [49]:

$$\mathcal{A}(E_s/N_0) = \int_0^1 \mathcal{E}(i, E_s/N_0)\, di, \qquad (30)$$

with i representing the mutual information ranging from $[0, 1]$ and $\mathcal{E}(i, E_s/N_0)$ is the EXIT curve at a given value of i and SNR.

Similarly, using the EXIT curves in Figure 5 the achievable rates of the MS-STSK systems considered associated with the DAC and the SAC configurations are shown in Figure 6.
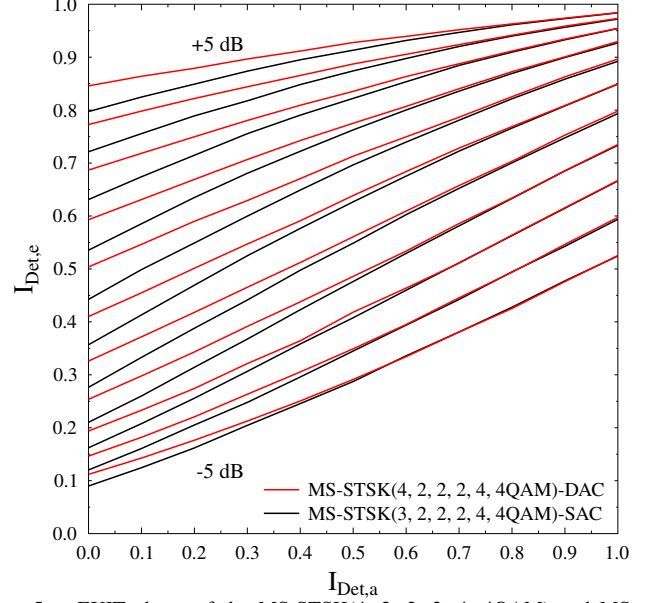

Figure 5. EXIT charts of the MS-STSK(4, 2, 2, 2, 4, 4QAM) and MS-STSK(3, 2, 2, 2, 4, 4QAM) systems associated with the DAC and SAC configurations, respectively.

Furthermore, the channel encoding rate directly affects the achievable rate due to the reduced effective transmission rate, hence the maximum achievable rate at a specific SNR value is given by [49]:

$$R_{max}(E_s/N_0) = R_{MS-STSK} \times R_c \times \mathcal{A}(E_s/N_0), \qquad (31)$$

where R_c is the outer decoder's achievable rate.

Using (31), the maximum achievable rates of the simulated systems having a half-rate RSC decoder are multiplied by $R_c = 1/2$, where the achievable rate of $R_{max} = 2.5$ bps/Hz of the DAC and SAC MS-STSK systems having $N_t = 4$ and $N_t = 3$ AEs is represented by the arrows in Figure 6 at SNR= -1.8 dB and -1.6 dB, respectively.

A summary of the achievable rates of the simulated systems associated with a half-rate RSC encoder are shown in Table II. It is clear from the table that by using the DAC configuration, higher number of transmit antennas is required than by using its SAC counterpart. Furthermore, the SNR values required for achieving the considered systems' achievable rates are enhanced by about 0.3 dB in most cases for the DAC configuration, which is indeed expected due to the higher number of AEs employed.

C. Convergence Behavior of the MS-STSK Scheme

To observe the convergence behavior of the MS-STSK system, we use the MS-STSK system having $R_{MS-STSK} = 5$ bpc, namely the DAC and SAC system given by the MS-STSK(4, 2, 2, 2, 4, 4QAM) and the MS-STSK(3, 2, 2, 2, 4, 4QAM) configurations associated with $\triangle\theta_c = 12.5°$, respectively.

The convergence behavior of the exchange of extrinsic information between the inner and the outer decoders, which is responsible of producing low error rates at a given SNR value, can be observed in the EXIT chart plots as follows.
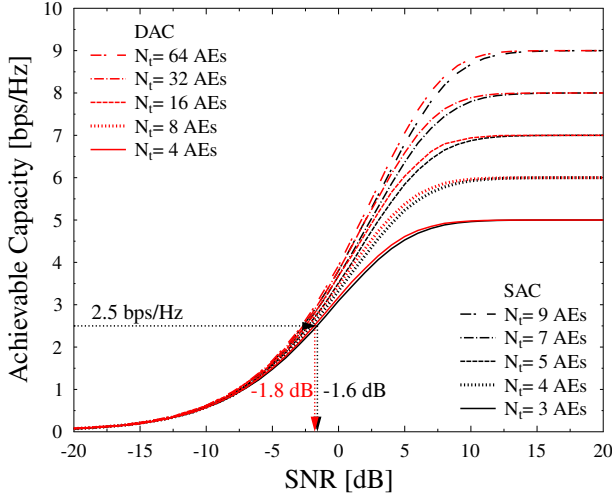
Figure 6. Maximum achievable limit of the MS-STSK(4, 2, 2, 2, 4, 4QAM), MS-STSK(8, 2, 2, 2, 4, 4QAM), MS-STSK(16, 2, 2, 2, 4, 4QAM), MS-STSK(32, 2, 2, 2, 4, 4QAM) and MS-STSK(64, 2, 2, 2, 4, 4QAM) systems associated with the DAC configuration as well as MS-STSK(3, 2, 2, 2, 4, 4QAM), MS-STSK(4, 2, 2, 2, 4, 4QAM), MS-STSK(5, 2, 2, 2, 4, 4QAM), MS-STSK(7, 2, 2, 2, 4, 4QAM) and MS-STSK(9, 2, 2, 2, 4, 4QAM) systems associated with the SAC configuration. Furthermore, the maximum achievable rate of the MS-STSK(4, 2, 2, 2, 4, 4QAM) system after employing a half-rate RSC decoder is shown at SNR= -1.8 dB, whereas the maximum achievable rate of the MS-STSK(3, 2, 2, 2, 4, 4QAM) system after employing a half-rate RSC decoder is shown at SNR= -1.6 dB.

$R_{\mathrm{MS-STSK}}$	N_t		R_{max}	SNR [dB]	
	DAC	SAC		DAC	SAC
5	4	3	2.5	-1.8	-1.6
6	8	4	3.0	-1.0	-0.7
7	16	5	3.5	-0.3	0.0
8	32	7	4.0	0.3	0.6
9	64	9	4.5	0.9	1.2

Table II
SUMMARY OF THE MAXIMUM ACHIEVABLE RATES OF THE SIMULATED SYSTEMS, WHERE THE SNR COLUMN REPRESENTS THE SNR VALUE REQUIRED TO ACHIEVE THE CAPACITY LIMIT.

In order to achieve a low BER, there has to be an open-tunnel between the inner and the outer decoder's EXIT curves, as shown in Figure 7. More specifically, the figure shows the EXIT curves of the MS-STSK(4, 2, 2, 2, 4, 4QAM) inner decoder at SNR=-3 dB to +2 dB and at -0.7 dB. Furthermore, Figure 7 portrays the EXIT chart of the half-rate RSC(2, 1, 4) decoder, where the representation of $I_{Dec,a}$ and $I_{Dec,e}$ is swapped between the x-axis and y-axis for ease of observation[1]. The open-tunnel shown between the inner curve at SNR=-0.7 dB and the outer curve allows the system to converge to a vanishingly low BER.
Furthermore, Figure 7 shows the convergence of the system at $SNR = -0.7$ dB using an input code length of 76,800 bits, where the output mutual information of $I_{Dec,e} = 1.0$ is reached after 11 iterations. Given that the steps shown in Figure 7 show the exchange of mutual information between

[1]**Please note that since the RSC decoder does not depend on the channel output, its EXIT curve is independent of the SNR value.**
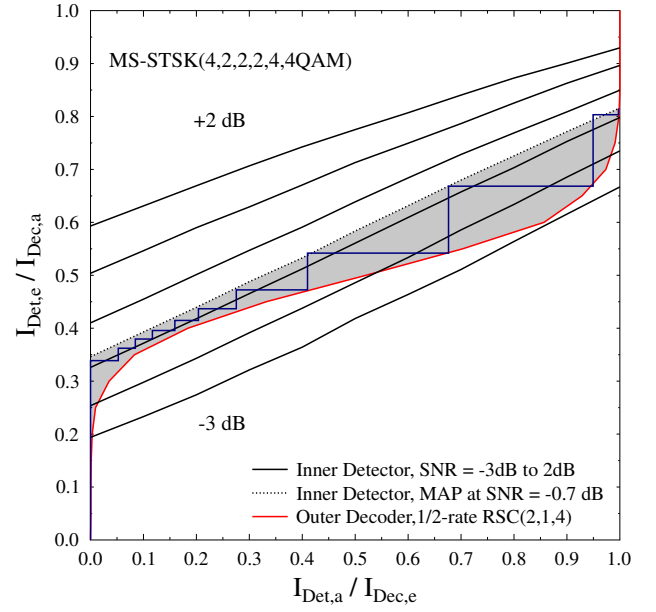

Figure 7. The EXIT charts of an MS-STSK(4, 2, 2, 2, 4, 4QAM) system associated with the DAC configuration. An open-tunnel is shown between the outer decoder's EXIT curve and the inner decoder's EXIT curve at SNR = -0.7 dB, where 11 iterations are required in order for the system to converge.

the inner and outer decoders, the convergence prediction based on the EXIT chart analysis is verified. Hence, the system is expected to produce an infinitesimally low BER at -0.7 dB, which is 1.1 dB away from the achievable capacity limit.
Furthermore, the convergence of the MS-STSK(3, 2, 2, 2, 4, 4QAM) system associated with the SAC configuration is shown in Figure 8. The stair-case-shaped Monte-Carlo decoding trajectory shown in the figure matches the EXIT chart-based convergence analysis, where the output mutual information of $I_{Dec,e} = 1.0$ is reached after 11 iterations and the system is expected to produce a vanishingly low BER at -0.2 dB, which is 1.4 dB away from the achievable capacity limit of -1.6 dB.
The EXIT tunnel of the SAC system shown in Figure 8 opens at 1.4 dB away from the maximum achievable rate, which is farther than the open-tunnel SNR of the DAC system, which becomes available at 1.1 dB away from the capacity in Figure 7. This is due to the reduced number of AEs, when applying the SAC configuration and owing to its additional system parameters that require further optimization, including the phase-shift and the specific AE allocation within each AC. For instance, allocating a single or multiple AEs in one or more AC would increase the inter-codeword correlation, which can severely affect the performance of the system. Hence, the detrimental effect of the inter-codeword correlation can be mitigated with the aid of an optimized phase-shift. Furthermore, the EXIT-tunnel area can be further reduced with the aid of enhanced channel codes, such as the family Irregular
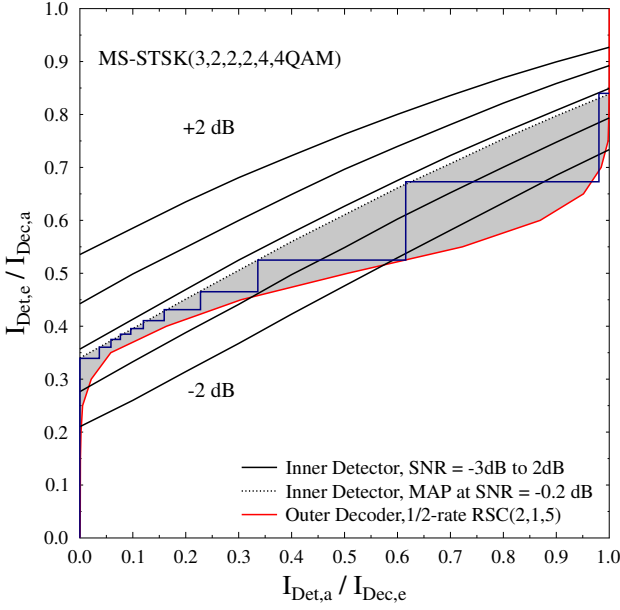
Figure 8. EXIT charts of an MS-STSK(3, 2, 2, 2, 4, 4QAM) system associated with the SAC configuration, where the open-tunnel is shown between the outer decoder's EXIT curve and the inner decoder's EXIT curve at SNR = -0.2 dB, which requires 11 iterations in order to converge.

Convolutional Codes (IrCC) [54], which can further shrink the open-tunnel area for the sake of reducing the capacity loss at the cost of an increased number of iterations, by carefully designing them in order for their EXIT curves to closely match the shape of the MS-STSK decoder. Similar trends are valid for the other considered MS-STSK systems associated with the DAC and the SAC configurations.

V. MS-STSK BER PERFORMANCE

In this section we use the previous system parameters of Section IV in order to verify the convergence behavior of the two systems considered. Figure 9 shows the BER performance of the MS-STSK(4, 2, 2, 2, 4, 4QAM) and the MS-STSK(3, 2, 2, 2, 4, 4QAM) systems associated with the DAC and SAC configurations, respectively. In both systems, the simulations were carried out using an input code length of 76,800 bits and a soft-decision decoder using 11 iterations. As expected from the convergence analysis of Section IV, the DAC system achieved a low BER at SNR= -0.7 dB, which is only 1.1 dB away from capacity. On the other hand, the SAC system produced a low BER at SNR= -0.2 dB, which is within 1.4 dB near of the capacity.

It is shown in Figure 9 that high BER values are achieved for both systems at SNR values lower than those shown in Figures 7 and Figure 8. This is due to the gradually closing tunnel at lower SNR values, where the intersection between the inner and outer decoder EXIT curves does not allow the decoder to converge.
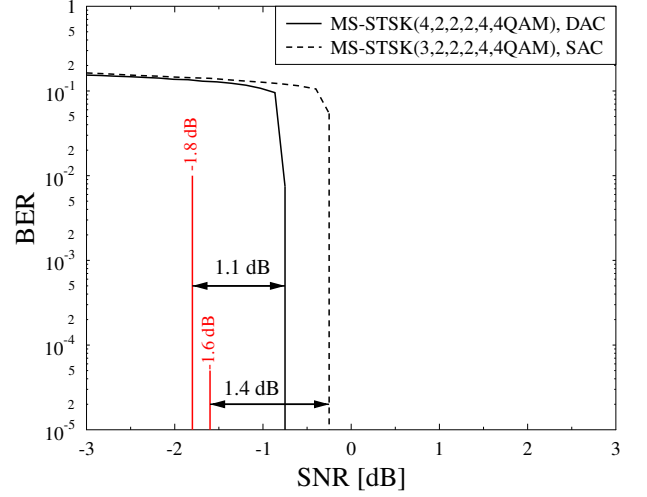

Figure 9. The BER performance of the MS-STSK(4, 2, 2, 2, 4, 4QAM) and the MS-STSK(3, 2, 2, 2, 4, 4QAM) systems associated with DAC and SAC configurations, respectively. The simulation was carried out using an input code length of 76,800 bits and a soft-decision decoder with 11 iterations for both systems.

VI. MS-STSK OVER WIDEBAND CHANNEL

It was shown in [21] that the MS-STSK scheme is capable of achieving both high diversity and multiplexing gains in narrow-band channels. In this section, we extend our scheme proposed in the previous section to operate over dispersive channels with the aid of the SC-FDE concept.

Figure 10 shows our MS-STSK coded transceiver architecture for both the OFDM and the SC-FDE structures. The dashed blocks belong only to the SC-FDE system, while the dotted blocks appear only in the OFDM scheme. Furthermore, the channel is assumed to inflict frequency selective fading, which would impose Inter-Symbol Interference (ISI) leading to performance degradation of the MS-STSK system.

A. OFDM-Aided MS-STSK

In OFDM, the system bandwidth is divided into N_{sc} non-dispersive sub-channels, where a frequency domain symbol is transmitted over each sub-channel. The transmitter and receiver structures are shown in Figure 10. The n_{sc}-th sub-carrier of the OFDM symbol carries the T_i-th time slot of the corresponding MS-STSK codeword, given that $T_i = 1, \ldots, T$ and $n_{sc} = 1, \ldots, N_{sc}$. Following the STSK OFDM frame generation advocated in [8], the entire $(N_t \times T)$-element MS-STSK codeword is transmitted over the same n_{sc}-th index over T time slots and the super-frame carrying all N_{sc} symbols is constructed as follows. The encoder shown in Figure 10 generates N_{sc} MS-STSK codewords using the coded bits arriving from the RSC encoder after being interleaved by the interleaver Π, in a similar approach to the process presented in Section III-B. Then, the ST mapper embedded in the MS-STSK encoder maps each of the T_i-th column of the n_{sc}-th codeword $\tilde{\mathbf{X}}(n_{sc}) = \tilde{A}_{q,c}(n_{sc}) s_l(n_{sc})$ into its corresponding MS-STSK n_{sc}-th index.
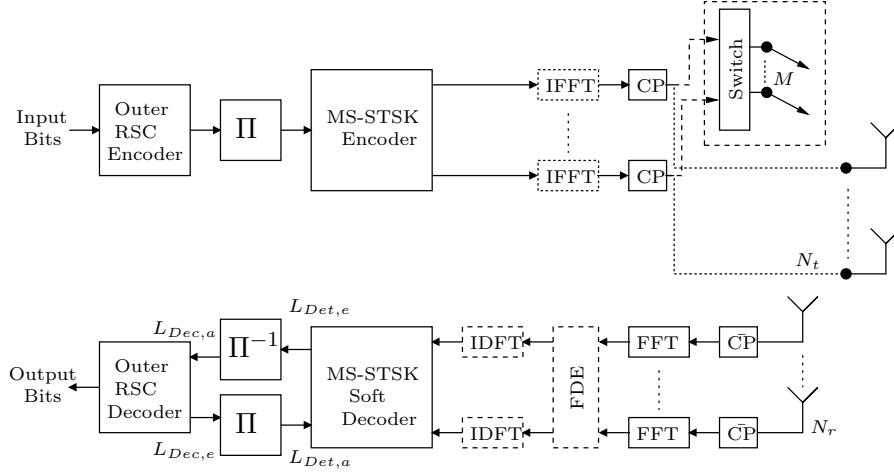
Figure 10. The OFDM/SC-FDE coded MS-STSK transceiver design. The dashed blocks are included in the SC-FDE scheme only and the dotted blocks appears only in the OFDM scheme.
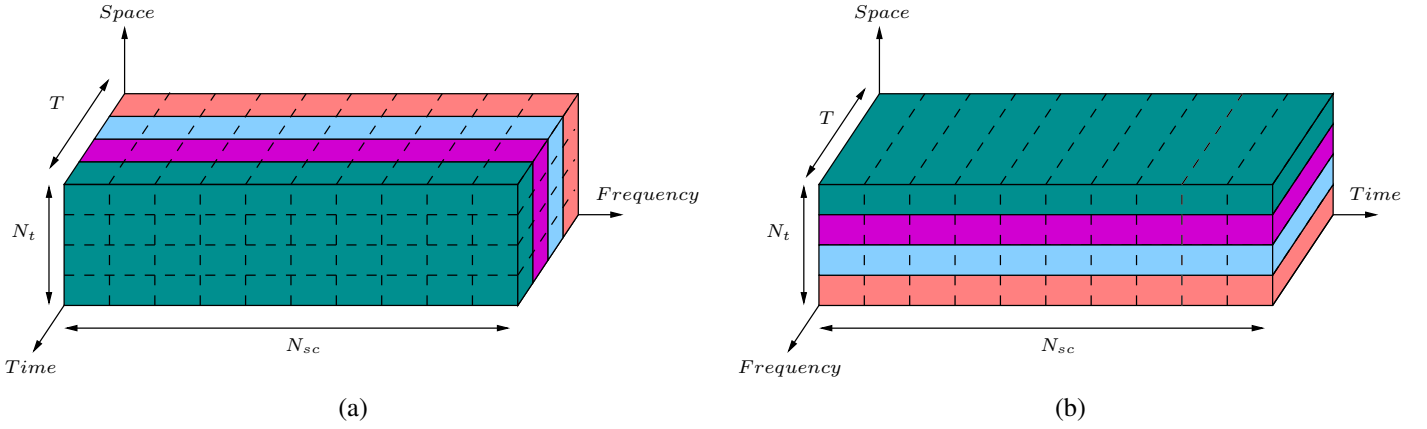

(a)

(b)

Figure 11. The T_i-th frame carrying the T_i-th column of all the N_{sc} MS-STSK generated codewords of the (a) transmitted OFDM frame (b) transmitted SC frame. The OFDM symbol's components are simultaneously transmitted over N_{sc} orthogonal sub-carriers, whilst the SC symbol's components are transmitted over N_{sc} time slots at a given carrier frequency.

The T_i-th frame carrying the T_i-th column of all the generated N_{sc} MS-STSK codewords is shown in Figure 11-(a) and can be written as

$$\mathbf{X}_{T_i} = [\tilde{\mathbf{X}}_{T_i}(1), \ldots, \tilde{\mathbf{X}}_{T_i}(N_{sc})] \in \mathbb{C}^{N_t \times N_{sc}}. \quad (32)$$

As shown in Figure 10, an IFFT operation is applied to each row of $\mathbf{X}_{T_i}$. Finally, the CP is added and the OFDM symbol shown in Figure 11-(a) is transmitted. Figure 11-(a) shows that the N_{sc} MS-STSK codewords generated are mapped to N_{sc} sub-carriers and transmitted over T OFDM symbols.

As shown in Figure 10, the CP is firstly removed and an FFT operation is applied to each of the signals received by each receive antenna. With the assumption of having a delay spread confined within the CP of the symbol, the symbol received at the n_{sc}-th sub-carrier and the T_i-th time slot after the FFT can be expressed as

$$\mathbf{Y}_{T_i}(n_{sc}) = \mathbf{H}(n_{sc})\tilde{\mathbf{X}}_{T_i}(n_{sc}) + \mathbf{V}_{n_{sc}}. \quad (33)$$

Given that the channel envelope encountered by the MS-STSK scheme is assumed to be constant over T time slots, the symbol

block received at the n_{sc}-th sub-carrier after T time slots can be expressed as

$$\mathbf{Y}(n_{sc}) = \mathbf{H}(n_{sc})\tilde{\mathbf{X}}(n_{sc}) + \tilde{\mathbf{V}}_{n_{sc}}. \quad (34)$$

Finally, the bits transmitted in the n_{sc}-th MS-STSK codeword can be detected using the soft-decision-aided detection of the symbol received at the n_{sc}-th sub-carrier, as detailed in Section III-B. The throughput of the full RF chain based OFDM scheme can be expressed as

$$R_{MS-STSK}^{(OFDM)} = \eta \cdot \log_2 \left(M_Q \cdot M_c \cdot N_c \right) \ (bits/symbol), \quad (35)$$

where η denotes the bandwidth efficiency expressed by [8]

$$\eta = \frac{N_{sc}}{(N_{sc} + N_{cp})}. \quad (36)$$

B. Challenges of OFDM-MSSTSK

In soft-decision-aided detection schemes invoking the Log-MAP algorithm [50], the detector relies on a soft-value representation of the received signal in order to indicate the level
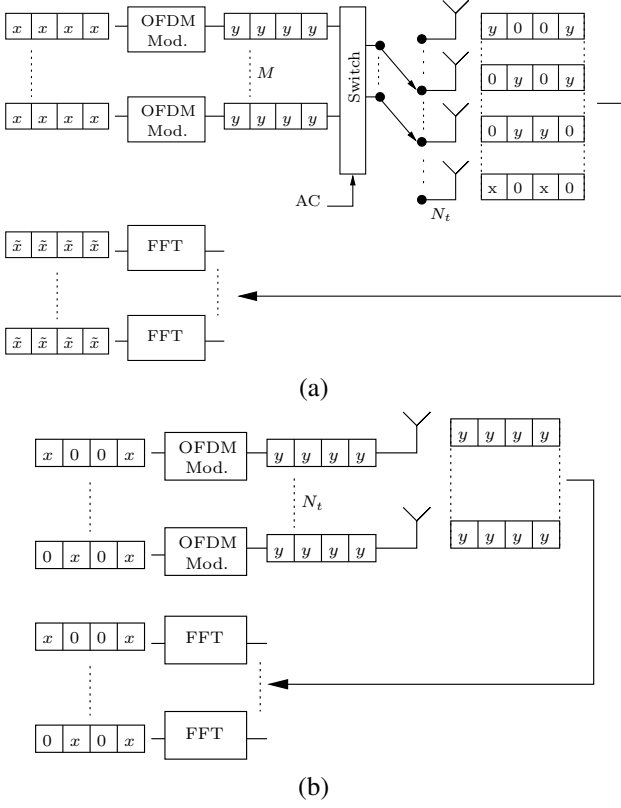
Figure 12. OFDM-based MS-STSK system representation with (a) Reduced RF chain (b) Full RF chain set.

of decision confidence. The transmitter of the OFDM-aided MS-STSK system requires the same number of RF chains as the total number of transmit antennas, yielding $N_{RF}= N_t$. Hence, the OFDM-aided system only benefits from the enhanced throughput of the MS-STSK scheme relying on a full RF chain solution [55], [56]. To further understand the effect of a reduced-RF-chain based OFDM system on a soft-decision-aided receiver, let us consider the pair of OFDM MS-STSK system representations seen in Figures 12 (a) and (b), where x, $\tilde{x}$ and y represent random values. In Figure 12(a), the MS-STSK system is equipped with $N_{RF}^t = M$ RF chains and $N_t > M$ AEs, where the OFDM modulation is applied prior to AC selection. The zeros appearing at the antenna output represent the inactive AEs at a specific sub-carrier, while the x symbols denote the transmitted symbols. At the receiver, the FFT operation employed would introduce a mismatch between the frequency domain signal produced and the pre-IFFT symbol of the transmitter due to the zeros padded in the received signal. In Figure 12(b), the MS-STSK system is equipped with equivalent numbers of RF chains and AEs, yielding $N_{RF}^t = N_t$. Here, the zeros referring to the inactive AEs at a specific sub-carrier are added prior to the OFDM modulation, where the time domain symbol is transmitted over all AEs. At the receiver, the inactive antenna elements can be observed at the post-FFT signal, hence the OFDM-based MS-STSK scheme requires a full-RF-chain based implementation.

However, in order to benefit from having a reduced number

of RF chain for our OFDM-based MS-STSK, the implicit information conveyed by the AC index should be transmitted per OFDM symbol. To achieve that, a single AC is activated to transmit an entire OFDM symbol divided into T time slots, while other TAs remain inactive, hence Equation (35) can be rewritten as

$$R_{MS-STSK}^{'(OFDM)} = \eta \cdot \log_2 (M_Q M_c) + \frac{\log_2 (N_c)}{N_{sc}} \ (bits/symbol),$$
$$(37)$$

where it is clearly shown that the throughput is substantially reduced, yielding $R_{MS-STSK}^{'(OFDM)} \lll R_{MS-STSK}^{(OFDM)}$. By contrast, an SC system would require only $N_{RF} = M$ RF chains, where the FDE is applied at the receiver side with the aid of a pair of DFT and IDFT operators and an equalizer, as shown in Figure 10.

C. SC-Aided MS-STSK

In the SC scheme, the MS-STSK codewords are transmitted over the time domain in order to overcome the impairment introduced by the dispersive channel, where no FFT operation is applied prior to transmission, as shown in Figure 10. Here, we use the same notation N_{sc} to refer to the total number of sub-carriers and time indices for the OFDM and SC-FDE schemes, respectively.

Both the SC-based and OFDM-based systems share the same MS-STSK codeword generation of $\tilde{\mathbf{X}}(n_{sc})$, given that the same index n_{sc} is used for denoting the sub-carrier index in the multi-carrier scheme and the time index in the SC scheme. The T_i-th component of all the time domain MS-STSK symbols mapped to the n_t-th TA can be expressed as:

$$\check{\mathbf{x}}_{n_t,T_i} = [x_{n_t,T_i}(1), \, x_{n_t,T_i}(2), \ldots, x_{n_t,T_i}(N_{sc})]^T, \quad (38)$$

where $\check{\mathbf{x}}_{n_t,T_i} \in \mathbb{C}^{N_{sc} \times 1}$ and $x_{n_t,T_i}(n_{sc})$ denotes the (n_t, T_i)-th component of the n_{sc}-th MS-STSK symbol $\mathbf{x}(n_{sc}) \equiv \tilde{\mathbf{X}}(n_{sc}) = \tilde{A}_{q,c}(n_{sc}) s_l(n_{sc})$. The T_i-th super-frame carrying all the T_i-th columns of all the N_{sc} MS-STSK codewords can be defined as

$$\check{\mathbf{x}}_{T_i} = [\check{\mathbf{x}}_{1,T_i} \ldots \check{\mathbf{x}}_{N_t,T_i}]^T, \quad (39)$$

where $\check{\mathbf{x}}_{T_i} \in \mathbb{C}^{N_{sc} N_t \times 1}$ and the overall SC-MS-STSK frame is expressed by

$$\check{\mathbf{x}} = [\check{\mathbf{x}}_1 \ldots \check{\mathbf{x}}_{T_i} \ldots \check{\mathbf{x}}_T]^T, \quad (40)$$

where $\check{\mathbf{x}} \in \mathbb{C}^{N_{sc} N_t \times T}$. Finally, the CP is concatenated to each $\check{\mathbf{x}}_{n_t,T_i}$ vector in (38) to get $\check{\mathbf{x}}'_{n_t,T_i} \in \mathbb{C}^{(N_{sc}+N_{cp}) \times 1}$ and the SC-MS-STSK frame $\check{\mathbf{x}}' \in \mathbb{C}^{(N_{sc}+N_{cp})N_t \times T}$ shown in Figure 11-(b) is transmitted over the dispersive channel. The SC symbol shown in Figure 11-(b) is transmitted over the same frequency component, but the codewords are separated by N_{sc} time-indices. Furthermore, as shown in Figure 10, the SC transmitter invokes a high-speed switch to map each n_{sc}-th column of $\check{\mathbf{x}}'_{T_i}$ to its assigned AC.

At the receiver of Figure 10, the CP is removed and an FFT operation is applied to each signal received at each antenna

in order to employ FDE. Assuming perfect synchronization at the receiver, the frequency domain representation of the N_{sc} received symbol matrix can be expressed as

$$\check{\mathbf{Y}} = \check{\mathbf{H}}\check{\mathbf{X}} + \check{\mathbf{V}}, \tag{41}$$

where $\check{\mathbf{H}} \in \mathbb{C}^{N_{sc}N_r \times N_{sc}N_t}$ is the frequency domain representation of the time domain $\tilde{H}$ with ξ-length CIRs, while $\check{\mathbf{V}}$ represents the AWGN. The channel $\check{\mathbf{H}}$ is formed of $(N_{sc} \times N_{sc})$-element sub-matrices $\check{\mathbf{H}}_{n_r,n_t} = \mathrm{diag}\{\check{h}_{n_r,n_t}(1),\ldots\check{h}_{n_r,n_t}(n_{sc}),\ldots,\check{h}_{n_r,n_t}(N_{sc})\}$, given that $\check{h}_{n_r,n_t}(n_{sc})$ is the corresponding n_{sc}-th component of the channel $\check{\mathbf{H}}_{n_r,n_t}$ of the n_t-th transmit antenna and of the n_r-th receive antenna, with $n_r = 1,\ldots,N_r$ being the receiver antenna index. Following the philosophy of [57], [58], FDE may be carried out with the aid of a combining matrix $\check{\mathbf{W}}$ using the ZF or the MMSE channel inversion techniques given by

$$\check{\mathbf{W}} = \begin{cases} \left(\check{\mathbf{H}}^H\check{\mathbf{H}}\right)\check{\mathbf{H}}^H, & ZF \\ \left(\check{\mathbf{H}}^H\check{\mathbf{H}} + \sigma_N^2\right)\check{\mathbf{H}}^H, & MMSE \end{cases} \tag{42}$$

and the frequency domain equalized symbol is represented by

$$\check{\mathbf{Z}} = \check{\mathbf{W}}\check{\mathbf{Y}}, \tag{43}$$
$$= \check{\mathbf{X}} + \check{\mathbf{V}}'. \tag{44}$$

Next, an IDFT operation is applied to the equalized symbol $\check{\mathbf{Z}}$. Hence, the symbol received at a given time index n_{sc} after T time slots can be expressed as

$$\check{\mathbf{z}}(n_{sc}) = \mathbf{x}(n_{sc}) + \check{\mathbf{v}}'(n_{sc}), \tag{45}$$

where as mentioned before, the n_{sc} denotes the time index of the SC system.

Then, the equalized symbol is fed into the soft-decision based MS-STSK detector of Figure 10, where following the soft-decision aided detector of Section III-B, the n_{sc}-th MS-STSK codeword can be detected under the assumption of an equalized channel in (17) as $\mathbf{H_c} = \mathcal{X}\mathcal{I}_c$ for the c-th AC. Hence, the soft-decision metric $\lambda_{q,l,c}$ in (27) can be rewritten as

$$\lambda_{q,l,c} = -\frac{\left\|\check{\mathbf{z}}(n_{sc}) - s_l\left(\bar{\mathbf{H}}_c\mathcal{X}\right)_q\right\|^2}{N_0} + \sum_{j\neq k} b_j L_a(b_j) \tag{46}$$

The throughput of the reduced-RF-chain based SC-FDE scheme can be expressed as

$$R_{MS-STSK}^{(SC-FDE)} = \eta \cdot \log_2\left(M_Q M_c N_c\right) \; (bits/symbol). \tag{47}$$

Observe by comparing (47) to (35) that the SC-FDE scheme benefits from both an enhanced throughput and an improved integrity for our MS-STSK scheme communicating over wideband channels relying on a reduced number of RF chains, as long as $\check{\mathbf{W}}$ of Equation (**42**) is not ill-conditioned and the system is not rank-deficient.
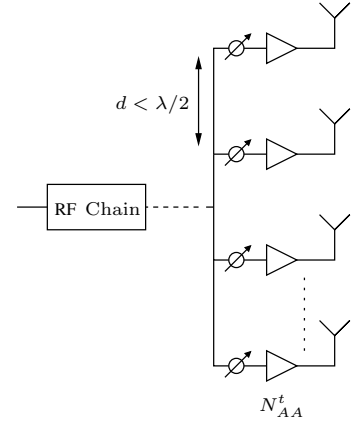

Figure 13.   Antenna array.

VII. SC-Based MS-STSK Scheme for Millimeter-Wave Systems

In this section, we employ the soft-decision-aided detectors proposed in Sections III-B and VI to MS-STSK systems operating at mmWaves.

Owing to the time dispersive and frequency selective nature of mmWave wideband channels [22], [30], [59], wideband techniques such as OFDM and SC-FDE have to be used for communication over the mmWave channel for the sake of mitigating the ISI imposed by the channel. However, due to the FFT impairments introduced by utilizing OFDM in SM, SC techniques are alternately adopted to benefit from the reduced-RF chain advantage of SM, as shown in Section VI. The mmWave channel is considered to be wideband due to the huge available bandwidths at each of its bands [60], which would require wideband modulation schemes for the sake of mitigating the effect of ISI.

As discussed in [14], SC-FDE has multiple advantages over OFDM. Given their comparable design complexity and performance, OFDM is less favourable at high frequencies due to its high PAPR and the more grave impairments introduced by the amplifier's non-linearity and the carrier frequency offset [26]. Furthermore, the OFDM-aided MS-STSK system requires a full RF chain based implementation, while the SC-FDE-aided scheme requires only $N_{RF} = M$ RF chains, which further reduces the cost of the MS-STSK transceiver. However, the SC-FDE scheme does not achieve its full potential with the aid of the low-complexity MMSE and ZF equalizers considered here. To achieve the best possible performance, the direct Minimum BER (MBER) equaliser of [61] would have to be employed.

Against this background, it is clear that the proposed MS-STSK transceiver can benefit from a reduced number of RF chains by employing SC-FDE rather than OFDM for mitigating the ISI. However, without employing beamforming, the system's performance would remain modest due to the mmWave signals' high path-loss. Hence, we replace each transmit and receiver AE used in Figure 3 by an antenna array (AA) in order to apply analogue beamforming (ABF), as shown in Figure 14. Each Transmit AA (TAA) and Receive AA (RAA) consist of N_{AA}^t and N_{AA}^r AEs, respectively, and

each AE is attached to a pair of phase-shifters and power amplifiers, where each AA requires a single RF chain. The transmitter is equipped with N_s TAAs, where the activated TAAs are connected to the available N_{RF}^t RF chains with aid of a high-speed switch, in order to transmit both the STSK codeword and the activated TAA index. The resultant MS-STSK scheme is now referred to as MS Steered STSK (MS-SSTSK), where the AAs employed at both sides are used for steering the signal with the aid of ABF.

Given that the mmWave channel is a clustered multipath channel [4], [62], where the multipath components arrive in distinct time-domain clusters and spatial lobes [22], the discrete-time CIR of the mmWave channel between the n_t-th transmit AE and the n_r-th receive AE may be expressed as [23]

$$\hat{h}_{n_t,n_r}(t,\tau) = \sum_{n_p=0}^{\bar{N}_p-1} h_{n_t,n_r}(t).\delta(\tau-\tau_{n_p}), \qquad (48)$$

where h_{n_t,n_r} represents the mmWave channel envelope and $\bar{N}_p = \sum_{n_c=1}^{N_{cl}} \sum_{n_p=1}^{N_p(n_c)} 1$ denotes the total number of multi-path components in all clusters, with N_{cl} being the total number of clusters and $N_p(n_c)$ the number of multi-path components in the n_{sc}-th cluster.

The input of the n_s-th TAA from the RF chain is transmitted on its N_{AA}^t AEs, as shown in Figure 13. But before that, ABF is applied at the n_t-th transmit antenna by a pair of phase-shifter and power amplifier by multiplying the n_{sc}-th symbol $x_{n_s,T_i}(n_{sc})$ assigned to the n_s-th TAA, shown in (38), by the ABF coefficient $w_{n_t,T_i}(n_{sc})$, which can be viewed as the multiplication of $x_{n_s,T_i}(n_{sc})$ by the ABF matrix $W_{n_s}(n_{sc}) \in \mathbb{C}^{1 \times N_{AA}^t}$, so that we have $W_{n_s}(n_{sc})^H W_{n_s}(n_{sc}) = I_{N_{AA}^t}$. Similarly, by using the AA of Figure 13 at the receiver side of Figure 10, ABF is applied at the n_{RF}^r-th RAA by multiplying the n_{sc}-th received symbols by the receive ABF matrix $P_{n_{RF}^r}(n_{sc}) \in \mathbb{C}^{N_{AA}^r \times 1}$, so that we have $P_{n_{RF}^r}(n_{sc})^H P_{n_{RF}^r}(n_{sc}) = I_{N_{AA}^r}$. Next, under the assumption of perfect synchronization at the receiver, the frequency domain representation of the received symbol matrix can be expressed by

$$\check{\mathbf{Y}} = \mathbf{P}\check{\mathbf{H}}_{\mathbf{w}}\mathbf{W}\check{\mathbf{X}} + \check{\mathbf{V}}, \qquad (49)$$

where, similar to (41), $\check{\mathbf{H}}_{\mathbf{w}} \in \mathbb{C}^{N_{sc}N_r \times N_{sc}N_t}$ is the frequency domain representation of the time domain $\tilde{H}_w$ associated with $\bar{N}_p$-length CIRs, while $\mathbf{W}$ and $\mathbf{P}$ denote the full transmit and receive ABF matrices at all time-slots, respectively.

The FDE operation is applied to the frequency domain channel using the effective channel, where the effective channel is the post-ABF channel expressed as $\mathbf{H_{eff}} = \mathbf{P}\check{\mathbf{H}}_{\mathbf{w}}\mathbf{W}$, which is assumed to be known at the receiver. After applying channel inversion using the techniques of (42), the frequency domain equalized symbol can be expressed as

$$\check{\mathbf{Z}} = a\check{\mathbf{X}} + \check{\mathbf{V}}', \qquad (50)$$

where a is a constant representing the beamforming gain, which under the idealized optimal ABF assumption can be expressed as $a = (N_{AA}^t N_{AA}^r)^{\frac{1}{2}}$ [8]. Next, the ABF gain would still appear after utilizing the IDFT and the received symbol at a given time index n_{sc} after T time slots can be expressed as

$$\check{\mathbf{z}}(n_{sc}) = a\mathbf{x}(n_{sc}) + \check{\mathbf{v}}'(n_{sc}). \qquad (51)$$

Finally, $\check{\mathbf{z}}(n_{sc})$ is fed into the soft-decision based MS-STSK detector of Figure 10, where the equalized channel of (17) is expressed as $\mathbf{H_c} = a\mathcal{X}\mathcal{I}_c$ for a given AC. The rest of the detection process is based on the soft-decision metric $\lambda_{q,l,c}$ of (46).

VIII. SC-BASED MS-SSTSK EXIT-CHART ANALYSIS AND BER PERFORMANCE

Based on the discussions in Sections VI and VII, the SC-based MS-STSK system of Figure 10 constitutes a better choice over an OFDM-based system for mmWaves in terms of its reduced number of RF chains. In this section, we use EXIT charts [49] for studying the behavior of our SC-FDE-aided MS-SSTSK of Figure 14 relying on a soft-decision based detector.

Consider a SC-FDE-aided MS-SSTSK scheme that employs MMSE for FDE and operates in the 28 GHz mmWave channel, where $N_s = 4$ TAAs and $N_{RF}^r = 4$ RAAs are employed at the transmitter and receiver sides, respectively. The system invokes an STSK(2, 2, 4, 4QAM) encoder associated with an SAC configuration in conjunction with a phase-shift rotation of $\phi = \pi/8$ per AC and $N_{AC} = 4$ ACs to achieve a throughput of $R_{MS-STSK}^{(SC-FDE)} = \log_2(4 \cdot 4 \cdot 4) = 6$ bits per codeword. The 28 GHz channel model employed is based on the channel measurements presented in [22], [23], where a block size of $N_{sc} = 1024$ is associated with a CP length of $N_{cp} = 100$.

Figure 15 shows the EXIT charts of the system considered at SNR values ranging from -5.0 dB to 5.0 dB with a step-size of 1.0 dB for each EXIT inner curve, where as stated in Section IV, $I_{Det,a}$ and $I_{Det,e}$ refer to the input and output mutual information of the soft-decision based MS-STSK detector, while $I_{Dec,a}$ and $I_{Dec,e}$ denote the input and output mutual information of the RSC decoder. Furthermore, Figure 15 also shows the EXIT curve of the outer RSC(2,1,4) channel encoder. As the SNR value increases, the inner decoder's EXIT chart is shifted upwards.

A. Maximum Achievable Rate

Again, the EXIT charts of the SC-FDE-aided MS-STSK system considered can be used for determining the maximum achievable rate of the system [49], where the area under the EXIT curve of the inner code $\mathcal{A}(E_s/N_0)$ can be used for determining the achievable rate of the system at a given SNR E_s/N_0 as $(1/2) \times R_{MS-STSK}^{(SC-FDE)} \times \mathcal{A}(E_s/N_0)$ bps/Hz. The maximum achievable limit of the SC-based MS-SSTSK system considered is shown in Figure 16, where the EXIT curves ranging from -20 dB to 15 dB are used for producing the achievable rate curve. Furthermore, when a half-rate RSC code is used for channel encoding, a system capacity limit of
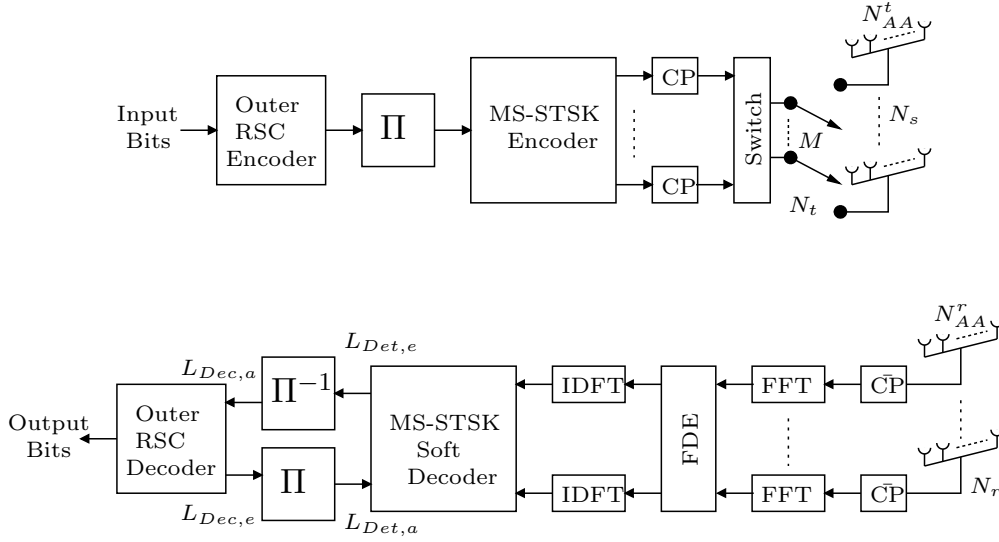
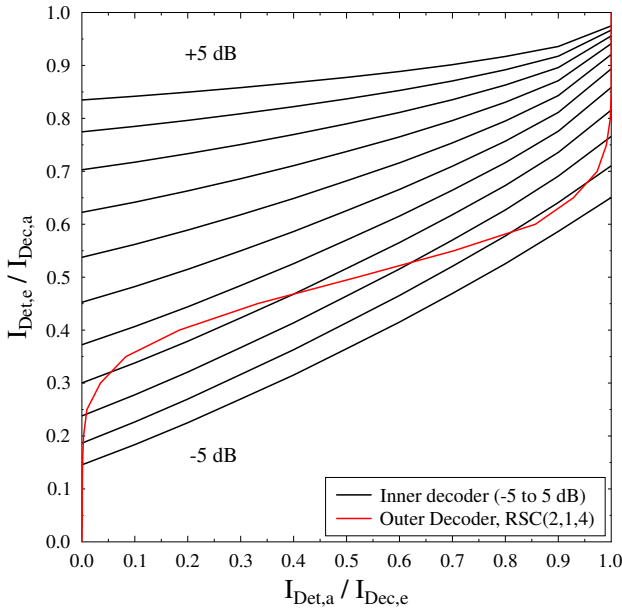Figure 14. The SC-FDE coded MS-SSTSK transceiver design.

Figure 15. EXIT charts of our SC-FDE-aided MS-SSTSK scheme over the 28 GHz mmWave channel, where a single-AE $N_s = 4$ and $N_{RF}^r = 4$ TAAs and RAAs are employed at the transmitter and receiver, respectively. Furthermore, the system invokes an STSK(2, 2, 4, 4QAM) encoder to achieve $N_{AC} = 4$ ACs with a phase-shift rotation of $\phi = \pi/8$ per AC.
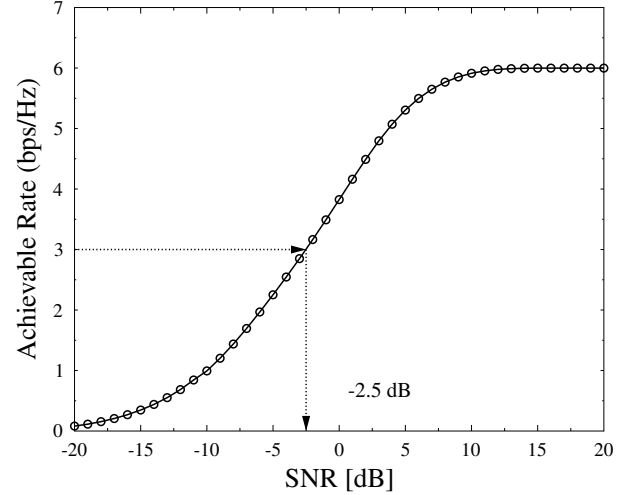

Figure 16. Maximum achievable limit of our SC-FDE-aided MS-SSTSK scheme over the 28 GHz mmWave channel, where a single-AE $N_s = 4$ and $N_{RF}^r = 4$ TAAs and RAAs are employed at the transmitter and the receiver, respectively. Furthermore, the system invokes an STSK(2, 2, 4, 4QAM) encoder to achieve $N_{AC} = 4$ ACs with a phase-shift of $\phi = \pi/8$ per AC.

3 bps/Hz can be achieved at $SNR = -2.5$ dB. Varying the number of TAAs and RF chains would shift the achievable rate according to the number of bits conveyed.

B. Convergence Behavior of the MS-SSTSK Scheme

The system parameters used for generating the simulation results of Figure 16 are adopted to observe the convergence behavior of the SC-based MS-SSTSK system. The EXIT curves of the system at $SNR = -1.4$ dB and of the outer RSC(2,1,4) decoder are shown in Figure 17, under the same assumptions of the wideband 28 GHz mmWave channel. Furthermore, the EXIT chart here is plotted using an input code length of 76,800 bits. An open tunnel is observed between the inner and outer decoder EXIT curves at -1.4 dB, where the output mutual information of $I_{Dec,e} = 1$ is reached after 14 iterations matching the EXIT chart-based convergence analysis. Hence, the system is expected to produce a low BER at -1.4 dB, which is only 1.1 dB away from the achievable capacity limit.

Figure 18. The BER performance of our SC-based MS-SSTSK scheme associated with MMSE channel equalization. By employing a half-rate RSC(2, 1, 4) channel encoder, the normalized throughput achieved is 3 bps/Hz, where the interleaver length used is 76800 bits with a block length of $N_{sc} = 1024$.
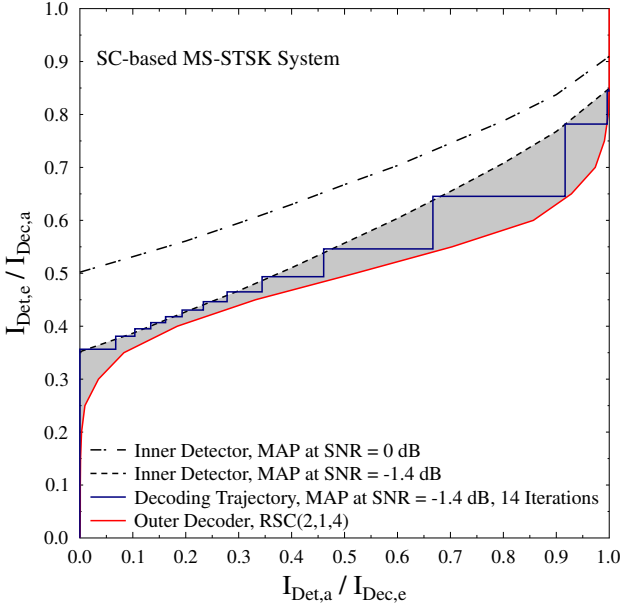
Figure 17. The EXIT charts of the SC-based MS-SSTSK system considered at -1.4 dB assuming a code length of 76800 bits. The convergence of the soft-decision detector is shown by the trajectory curve in the open tunnel between the RSC decoder and the MS-STSK detector EXIT charts.

C. SC-Based MS-SSTSK BER performance

The previous system parameters used above and the mmWave channel are used in our simulations. In Figure 18, we characterize the achievable BER performance of the SC-based MS-SSTSK system presented in Figure 17 relying on the soft-decision detector associated with 14 iterations at SNR= -1.4 dB. The BER curve shown in Figure 19 matches our earlier analysis, the system is capable of achieving a low BER at the desired SNR value with the aid of 14 iterations, which is within 1.1 dB of the capacity.

Furthermore, more AEs can be employed at each of the TAAs and RAAs to achieve SNR gains with the aid of both transmit and receive ABF, which are crucial for overcoming the high mmWave path-losses. Figure 19 shows the effect of adding more AEs to either the transmitter or the receiver, where with the assistance of an optimal ABF, an extra 6 dB and 12 dB gain can be achieved for a configuration of $(N_{AA}^t, N_{AA}^r) = (2, 2)$ and $(2, 8)$ AEs, which can be translated to shifting the curves of Figure 17 by 6 dB and 12 dB, respectively as shown in [8].
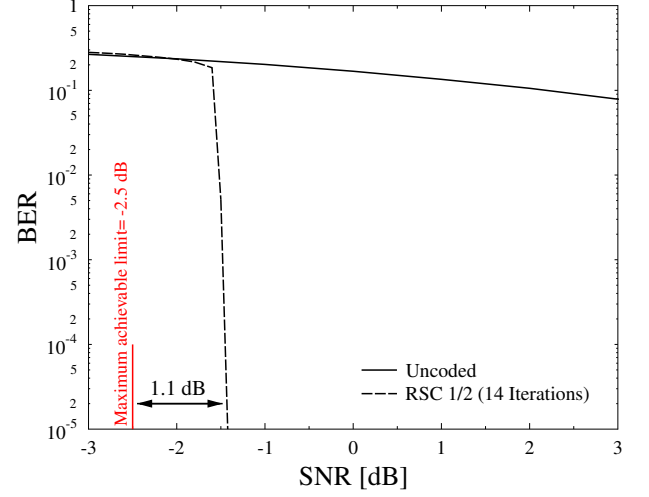

Figure 19. The BER performance of our SC-based MS-SSTSK scheme associated with MMSE channel equalization. By employing a half-rate RSC(2, 1, 4) channel encoder, the normalized throughput achieved is 3 bps/Hz, where the interleaver length used is 76800 bits with a block length of $N_{sc} = 1024$. Furthermore, the figure shows the BER performance of the SC-based MS-SSTSK scheme associated with MMSE channel equalization and $(N_{AA}^t, N_{AA}^r) = (2, 2)$ and $(2, 8)$ AEs configuration.

IX. DESIGN GUIDELINES

The MS-STSK scheme has the potential of outperforming other MIMO arrangements, such as the Orthogonal Space-Time Block Code (OSTBC), V-BLAST, SM, LDC and STSK schemes, provided that the MS-STSK's parameters are appropriately selected. A summary of the complexity order, diversity order[2], data rate and required number of RF chains of the

[2]Diversity order achieved using spatial diversity.

aforementioned MIMO arrangements compared to the MS-STSK scheme is shown in Table III.

For example, let us consider a system, where we have two RF chains at the transmitter, with the exception of SM having a single RF chain. Furthermore, let us assume having two antenna elements at the receiver, while we use $M_Q = 2$ and $T = 2$, when required. Given that we aim for a throughput of 4 bpc, a summary of all the OSTBC, V-BLAST, SM, LDC,

Scheme	Complexity	Diversity	Rate	RF Chains
OSTBC [63]	$\mathcal{O}(M_c)$	$(N_t \cdot N_r)$	$\leq \log_2(M_c)$	N_t
V-BLAST [64]	$\mathcal{O}(M_c^{N_t})$	$(N_t - N_r + 1)$	$\log_2(M_c \cdot N_t)$	N_t
SM [10], [11]	$\mathcal{O}(N_t M_c)$	N_r	$\log_2(N_t \cdot M_c)$	1
LDC [65]	$\mathcal{O}(N_t \cdot M_c)^{M_Q}$	$N_r \cdot \min(M, T)$	$M_Q \cdot \log_2(N_t \cdot M_c)/T$	$N_t = M$
STSK [17]	$\mathcal{O}(M_Q M_c)$	$N_r \cdot \min(M, T)$	$\log_2(M_Q \cdot M_c)/T$	$N_t = M$
MS-STSK [21]	$\mathcal{O}(M_Q M_c N_c)$	$N_r \cdot \min(M, T)$	$\log_2(M_Q \cdot M_c \cdot N_c)/T$	$M < N_t$

Table III

A SUMMARY OF THE COMPLEXITY ORDER, DIVERSITY ORDER AND DATA RATE OF VARIOUS MIMO ARRANGEMENTS, NAMELY THE OSTBC, V-BLAST, SM, LDC, STSK AND MS-STSK SCHEMES.

STSK and MS-STSK[3] system configurations is provided in Table IV. To expound a little further, the OSTBC, V-BLAST and SM systems impose a lower complexity order than that of the LDC, STSK and MS-STSK systems, which have identical complexity orders, as shown Table IV. Furthermore, excluding the V-BLAST and SM schemes, which achieve diversity orders of one and two, respectively, all other systems achieve the same diversity order of four. Accordingly, the number of RF chains is considered to be equal to the number of transmit AEs of two for all systems, except for conventional SM and MS-STSK, where SM is associated with a single RF-chain and two transmit AEs, while MS-STSK is associated with two RF-chains and seven transmit AEs[4].

It was demonstrated in [11], [66], [67] that the SM/SSK scheme is capable of outperforming the V-BLAST and OS-TBC. Furthermore, Sugiura *et al.* investigated the performance of STSK in comparison to many other MIMO schemes, such as V-BLAST, SM and LDC in [17] and [18], where it was factually shown that STSK is capable of outperforming these systems, despite imposing a lower detection complexity order. Additionally, it was shown in [21] that MS-STSK is capable of outperforming STSK, hence, MS-STSK has the potential of outperforming the conventional MIMO schemes, such as the ones considered in this example, which can be ensured by carefully choosing the MS-STSK's parameters, namely the number of RF-chains, M_Q and M_c.

In Table V, we show the design trade-offs between the DAC and the SAC implementations of the MS-STSK scheme. Given that the DAC requires a unique AE set for each AC, the throughput of the system is typically reduced, since not all the available ACs are invoked. However, the uniqueness of the DAC's ACs allows us to achieve the full diversity order of the MS-STSK system formulated in Table III, whereas due to the AE sharing in the SAC, preprocessing is required in order to achieve the full diversity order. Furthermore, relying on the same number of RF chains for both allocation techniques, an MS-STSK system associated with the DAC arrangement would require more AEs in order to achieve the same throughput than the SAC arrangement.

Furthermore, a soft-decision-aided MS-STSK decoder can be introduced relying on iterative two-stage serially concatenated inner and outer decoders that exchange extrinsic information

in order to attain near-capacity performance. More specifically, the system was capable of achieving a performance within 1.1 dB and 1.4 dB from the capacity limit of the DAC and SAC configurations, respectively.

For the sake of transmitting over the mmWave wideband channel, the proposed soft-decision aided MS-STSK system can be combined both with OFDM and with SC-FDE techniques. Additionally, the system can be combined with ABF for the sake of mitigating the path-loss of mmWaves. However, the SC-based structure is preferrable over its OFDM-based counterpart since it is capable of retaining the benefit of having a reduced number of RF-chains for the MS-STSK scheme. The proposed soft-decision SC-based MS-STSK system associated with ABF is capable of operating over dispersive mmWave channels, while achieving a performance within 1.1 dB of the capacity limit. We summarize the complexity order, diversity order and data rate of the MS-STSK scheme and its wideband SC-FDE and OFDM arrangements in Table VI. Therefore, the design guidelines of the systems proposed in this treatise can be summarised as follows:

- By suitably choosing the MS-STSK parameters, our sophisticated MIMO arrangement has the potential of outperforming other MIMO arrangements, upon ;
- The two-stage serially concatenated soft-decision-aided MS-STSK detector of Figure 4 has to rely on soft-decisions for the sake of further enhancing the hard-decision MS-STSK system when aiming for near-capacity performance;
- The MS-STSK system has to be amalgamated with OFDM or SC-FDE in order to operate over wideband channels.
- Moreover, employing ABF is essential for transmitting over the mmWave channel;
- We opt for the amalgam of MS-STSK, SC-FDE and analogue beamforming for communicating over the mmWave channel and drop that with the OFDM for the sake of exploiting the key advantages of MS-STSK, namely its enhanced performance, throughput as well as its reduced complexity order, while preserving its reduced RF-chain advantage.

X. CONCLUSIONS

In this paper we presented a soft-decision aided MS-SSTSK decoder relying on iterative two-stage serially concatenated inner and outer decoders that exchange extrinsic information

---

[3]MS-STSK is assumed to be associated with the SAC.

[4]MS-STSK associated with the SAC configuration requires seven transmit AEs to achieve $N_c = 16$ given that $M = 2$.

Scheme	Complexity	Diversity	Rate	RF Chains
OSTBC	$\mathcal{O}\left(16\right)=\mathcal{O}\left(16\right)$	$\left(2\cdot 2\right)=4$	$\leq \log_2\left(16\right)=4$	$N_t=2$
V-BLAST	$\mathcal{O}\left(8^2\right)=\mathcal{O}\left(64\right)$	$\left(2-2+1\right)=1$	$\log_2\left(8\cdot 2\right)=4$	$N_t=2$
SM	$\mathcal{O}\left(2\cdot 8\right)=\mathcal{O}\left(16\right)$	$N_r=2$	$\log_2\left(2\cdot 8\right)=4$	1
LDC	$\mathcal{O}\left(4^4\right)=\mathcal{O}\left(256\right)$	$2\cdot \min\left(2,2\right)=4$	$4\cdot \log_2\left(4\right)/2=4$	$N_t=2$
STSK	$\mathcal{O}\left(4\cdot 64\right)=\mathcal{O}\left(256\right)$	$2\cdot \min\left(2,2\right)=4$	$\log_2\left(4\cdot 64\right)/2=4$	$N_t=2$
MS-STSK	$\mathcal{O}\left(4\cdot 4\cdot 16\right)=\mathcal{O}\left(256\right)$	$2\cdot \min\left(2,2\right)=4$	$\log_2\left(4\cdot 4\cdot 16\right)/2=4$	$\left(M=2\right)<$ $\left(N_t=7\right)$

Table IV

AN EXAMPLE OF A SYSTEM HAVING TWO RF CHAINS - WITH AN EXCEPTION OF SM HAVING A SINGLE RF CHAIN - AND TWO RECEIVE ANTENNA ELEMENTS AS WELL AS M_Q AND $T=2$ WHEN NECESSARY.

AC Allocation	DAC	$<,>,=$	SAC
Throughput	Reduced Throughput (Due to AC Uniqueness)	$<$	Enhanced Throughput (Due to AE Sharing)
Diversity	Full diversity (No Inter-Codeword Correlation)	$\geq$	Requires Optimization (Inter-Codeword Correlation)
Performance	Better Performance	$>$	Requires Optimization
RF Chains	M	$=$	M
AEs	N_t	$>$	N_t

Table V

THE DAC VERSUS THE SAC DESIGN TRADE-OFFS.

Scheme	Complexity	Diversity	Rate	RF Chains
MS-STSK [21]	$\mathcal{O}(M_Q\cdot M_c\cdot N_c)$	$N_r\cdot \min\left(M,T\right)$	$\log_2\left(M_Q\cdot M_c\cdot N_c\right)/T$	$M<N_t$
OFDM MS-STSK [56]	$\mathcal{O}(M_Q\cdot M_c\cdot N_c)$	$N_r\cdot \min\left(M,T\right)$	$\eta\log_2\left(M_Q\cdot M_c\cdot N_c\right)/T$	$M=N_t$
SC-FDE MS-STSK	$\mathcal{O}(M_Q\cdot M_c\cdot N_c)$	$N_r\cdot \min\left(M,T\right)$	$\eta\log_2\left(M_Q\cdot M_c\cdot N_c\right)/T$	$M<N_t$

Table VI

A SUMMARY OF THE COMPLEXITY ORDER, DIVERSITY ORDER AND DATA RATE OF THE MS-STSK SCHEME AND ITS SC-FDE AND OFDM ARRANGEMENTS.

in order to attain near-capacity performance. The MS-STSK system associated with our DAC and SAC configurations was analyzed and its achievable rates were evaluated using EXIT charts. The system was capable of achieving a performance within 1.1 dB and 1.4 dB from the capacity limit for the DAC and SAC configurations, respectively. Furthermore, the proposed soft-decision MS-STSK system was combined with OFDM and SC-FDE techniques in order to operate over wideband channels and with ABF for the sake of mitigating the path-loss of mmWaves. Additionally, we opted for the SC-based structure in order to maintain the benefit of having a reduced number of RF-chains for our MS-STSK scheme. The proposed soft-decision SC-based MS-SSTSK system associated with ABF is capable of operating over the dispersive mmWave channels, while achieving a performance within 1.1 dB of the capacity limit.

REFERENCES

[1] F. Khan and Z. Pi, "mmwave Mobile Broadband (MMB): Unleashing The 3-300GHz Spectrum," in *Sarnoff Symposium, 34th IEEE*, May 2011, pp. 1–6.

[2] Z. Pi and F. Khan, "System Design and Network Architecture for a Millimeter-wave Mobile Broadband (MMB) System," in *Sarnoff Symposium, 34th IEEE*, May 2011, pp. 1–6.

[3] L. Hanzo, H. Haas, S. Imre, D. O'Brien, M. Rupp, and L. Gyongyosi, "Wireless Myths, Realities, and Futures: From 3G/4G to Optical and Quantum Wireless," *Proceedings of the IEEE*, vol. 100, no. Special Centennial Issue, pp. 1853–1888, May 2012.

[4] T. Rappaport, S. Sun, R. Mayzus, H. Zhao, Y. Azar, K. Wang, G. Wong, J. Schulz, M. Samimi, and F. Gutierrez, "Millimeter Wave Mobile Communications for 5G Cellular: It Will Work!" *IEEE Access*, vol. 1, pp. 335–349, 2013.

[5] W. Roh, J.-Y. Seol, J. Park, B. Lee, J. Lee, Y. Kim, J. Cho, K. Cheun, and F. Aryanfar, "Millimeter-Wave Beamforming as an Enabling Technology for 5G Cellular Communications: Theoretical Feasibility and Prototype Results," *Communications Magazine, IEEE*, vol. 52, no. 2, pp. 106–113, February 2014.

[6] A. Adhikary, E. Al Safadi, M. Samimi, R. Wang, G. Caire, T. Rappaport, and A. Molisch, "Joint Spatial Division and Multiplexing for mm-Wave Channels," *IEEE Journal on Selected Areas in Communications*, vol. 32, no. 6, pp. 1239–1255, June 2014.

[7] L. Hanzo, M. El-Hajjar, and O. Alamri, "Near-Capacity Wireless Transceivers and Cooperative Communications in the MIMO Era: Evolution of Standards, Waveform Design, and Future Perspectives," *Proceedings of the IEEE*, vol. 99, no. 8, pp. 1343–1385, Aug 2011.

[8] I. A. Hemadeh, M. El-Hajjar, S. Won, and L. Hanzo, "Layered Multi-Group Steered Space-Time Shift-Keying for Millimeter-Wave Commu-

nications," *IEEE Access*, vol. 4, pp. 3708–3718, 2016.

[9] O. El Ayach, S. Rajagopal, S. Abu-Surra, Z. Pi, and R. Heath, "Spatially Sparse Precoding in Millimeter Wave MIMO Systems," *IEEE Transactions on Wireless Communications*, vol. 13, no. 3, pp. 1499–1513, March 2014.

[10] Y. A. Chau and S.-H. Yu, "Space Modulation on Wireless Fading Channels," in *Vehicular Technology Conference (VTC) Fall. IEEE VTS 54th*, vol. 3, 2001, pp. 1668–1671 vol.3.

[11] R. Mesleh, H. Haas, S. Sinanovic, C. W. Ahn, and S. Yun, "Spatial Modulation," *IEEE Transactions on Vehicular Technology*, vol. 57, no. 4, pp. 2228–2241, July 2008.

[12] C. Xu, S. Sugiura, S. X. Ng, and L. Hanzo, "Spatial Modulation and Space-Time Shift Keying: Optimal Performance at a Reduced Detection Complexity," *IEEE Transactions on Communications*, vol. 61, no. 1, pp. 206–216, January 2013.

[13] H. Men and M. Jin, "A Low-Complexity ML Detection Algorithm for Spatial Modulation Systems With M-PSK Constellation," *IEEE Communications Letters*, vol. 18, no. 8, pp. 1375–1378, Aug 2014.

[14] S. Sugiura and L. Hanzo, "Single-RF Spatial Modulation Requires Single-Carrier Transmission: Frequency-Domain Turbo Equalization for Dispersive Channels," *IEEE Transactions on Vehicular Technology*, vol. 64, no. 10, pp. 4870–4875, Oct 2015.

[15] P. Yang, M. D. Renzo, Y. Xiao, S. Li, and L. Hanzo, "Design Guidelines for Spatial Modulation," *IEEE Communications Surveys and Tutorials*, vol. 17, no. 1, pp. 6–26, First Quarter 2015.

[16] C. Masouros and L. Hanzo, "Constellation Randomization Achieves Transmit Diversity for Single-RF Spatial Modulation," *IEEE Transactions on Vehicular Technology*, vol. 65, no. 10, pp. 8101–8111, Oct 2016.

[17] S. Sugiura, S. Chen, and L. Hanzo, "Space-Time Shift Keying: A Unified MIMO Architecture," in *IEEE Global Telecommunications Conference*, Dec 2010, pp. 1–5.

[18] ——, "Coherent and Differential Space-Time Shift Keying: A Dispersion Matrix Approach," *IEEE Transactions on Communications*, vol. 58, no. 11, pp. 3219–3230, November 2010.

[19] J. Wang, S. Jia, and J. Song, "Generalised Spatial Modulation System with Multiple Active Transmit Antennas and Low Complexity Detection Scheme," *IEEE Transactions on Wireless Communications*, vol. 11, no. 4, pp. 1605–1615, April 2012.

[20] S. Sugiura, C. Xu, S. X. Ng, and L. Hanzo, "Reduced-Complexity Iterative-Detection-Aided Generalized Space-Time Shift Keying," *IEEE Transactions on Vehicular Technology*, vol. 61, no. 8, pp. 3656–3664, Oct 2012.

[21] I. A. Hemadeh, M. El-Hajjar, S. Won, and L. Hanzo, "Multi-Set Space-Time Shift-Keying With Reduced Detection Complexity," *IEEE Access*, vol. 4, pp. 4234–4246, 2016.

[22] M. Samimi and T. Rappaport, "Ultra-Wideband Statistical Channel Model for Non Line of Sight Millimeter-Wave Urban Channels," in *Global Communications Conference (GLOBECOM), IEEE*, Dec 2014, pp. 3483–3489.

[23] M. K. Samimi and T. S. Rappaport, "3-D Statistical Channel Model For Millimeter-Wave Outdoor Mobile Broadband Communications," in *International Conference on Communications (ICC), IEEE*, June 2015, pp. 2430–2436.

[24] ——, "Local Multipath Model Parameters for Generating 5G Millimeter-Wave 3GPP-Like Channel Impulse Response," in *10th European Conference on Antennas and Propagation (EuCAP)*, April 2016, pp. 1–5.

[25] C. Gustafson, K. Haneda, S. Wyne, and F. Tufvesson, "On mm-Wave Multipath Clustering and Channel Modeling," *IEEE Transactions on Antennas and Propagation*, vol. 62, no. 3, pp. 1445–1455, March 2014.

[26] L. Hanzo, M. Münster, B. Choi, and T. Keller, *OFDM and MC-CDMA for Broadband Multi-user Communications, WLANs and Broadcasting*. John Wiley & Sons, May 2003. [Online]. Available: http://eprints.soton.ac.uk/258228/

[27] D. Falconer, S. L. Ariyavisitakul, A. Benyamin-Seeyar, and B. Eidson, "Frequency Domain Equalization For Single-Carrier Broadband Wireless Systems," *IEEE Communications Magazine*, vol. 40, no. 4, pp. 58–66, Apr 2002.

[28] S. Hur, T. Kim, D. Love, J. Krogmeier, T. Thomas, and A. Ghosh, "Millimeter Wave Beamforming for Wireless Backhaul and Access in Small Cell Networks," *IEEE Transactions on Communications*, vol. 61, no. 10, pp. 4391–4403, October 2013.

[29] S. Kutty and D. Sen, "Beamforming for Millimeter Wave Communications: An Inclusive Survey," *IEEE Communications Surveys Tutorials*, vol. 18, no. 2, pp. 949–973, Secondquarter 2016.

[30] T. Rappaport, G. Maccartney, M. Samimi, and S. Sun, "Wideband Millimeter-Wave Propagation Measurements and Channel Models for Future Wireless Communication System Design," *IEEE Transactions on Communications*, vol. 63, no. 9, pp. 3029–3056, Sept 2015.

[31] C. Kim, J.-S. Son, T. Kim, and J.-Y. Seol, "on The Hybrid Beamforming With Shared Array Antenna for Mmwave MIMO-OFDM Systems," in *Wireless Communications and Networking Conference (WCNC), IEEE*, April 2014, pp. 335–340.

[32] S. Ganesan, R. Mesleh, H. Ho, C. W. Ahn, and S. Yun, "On the Performance of Spatial Modulation OFDM," in *2006 Fortieth Asilomar Conference on Signals, Systems and Computers*, Oct 2006, pp. 1825–1829.

[33] T. Rappaport, J. Murdock, and F. Gutierrez, "State of the Art in 60-GHz Integrated Circuits and Systems for Wireless Communications," *Proceedings of the IEEE*, vol. 99, no. 8, pp. 1390–1436, Aug 2011.

[34] P. Yang, Y. Xiao, Y. L. Guan, K. V. S. Hari, A. Chockalingam, S. Sugiura, H. Haas, M. D. Renzo, C. Masouros, Z. Liu, L. Xiao, S. Li, and L. Hanzo, "Single-Carrier SM-MIMO: A Promising Design for Broadband Large-Scale Antenna Systems," *IEEE Communications Surveys Tutorials*, vol. 18, no. 3, pp. 1687–1716, thirdquarter 2016.

[35] C. Shannon, "A Mathematical Theory of Communication," *Bell System Technical Journal*, vol. 27, 1948.

[36] R. W. Hamming, "Error-Detecting And Error-Correcting Codes," *Bell System Technical Journal*, vol. 29, pp. 41–56, 1950.

[37] P. Elias, "Coding for Noisy Channels," *IRE Conv. Rept.*, pp. 37–47, 1955.

[38] C. Berrou and A. Glavieux, "Near Optimum Error Correcting Coding And Decoding: Turbo-Codes," *IEEE Transactions on Communications*, vol. 44, no. 10, pp. 1261–1271, Oct 1996.

[39] L. Hanzo, T. Liew, and B. Yeap, *Turbo Coding, Turbo Equalisation and Space-Time Coding for Transmission over Fading Channels*. Wiley, 2002. [Online]. Available: http://books.google.co.uk/books?id=3mOhrvMWTwQC

[40] L. Bahl, J. Cocke, F. Jelinek, and J. Raviv, "Optimal Decoding of Linear Codes for Minimizing Symbol Error Rate," *IEEE Transactions on Information Theory*, vol. 20, no. 2, pp. 284–287, Mar 1974.

[41] S. Benedetto and G. Montorsi, "Iterative Decoding of Serially Concatenated Convolutional Codes," *Electronics Letters*, vol. 32, no. 13, pp. 1186–1188, Jun 1996.

[42] L. Hanzo, T. Liew, B. Yeap, R. Tee, and S. Ng, *Turbo Coding, Turbo Equalisation and Space-Time Coding: EXIT-Chart-Aided Near-Capacity Designs for Wireless Channels*. Wiley, 2011. [Online]. Available: https://books.google.co.uk/books?id=i0gRC0wGVFgC

[43] S. T. Brink, "Convergence Behavior of Iteratively Decoded Parallel Concatenated Codes," *IEEE Transactions on Communications*, vol. 49, no. 10, pp. 1727–1737, Oct 2001.

[44] Abhishek, S. Kumar, and S. Chakrabarti, "Performance Evaluation of Asymmetric Turbo Codes Using Log-MAP Decoding Technique," in *International Conference on Devices and Communications (ICDeCom)*, Feb 2011, pp. 1–5.

[45] M. I. Kadir, S. Chen, K. Hari, K. Giridhar, and L. Hanzo, "OFDM-Aided Differential Space-Time Shift Keying Using Iterative Soft Multiple-Symbol Differential Sphere Decoding," *IEEE Transactions on Vehicular Technology*, vol. 63, no. 8, pp. 4102–4108, Oct 2014.

[46] M. Kadir, S. Sugiura, S. Chen, and L. Hanzo, "Unified MIMO-Multicarrier Designs: A Space-Time Shift Keying Approach," *Communications Surveys Tutorials, IEEE*, vol. 17, no. 2, pp. 550–579, Secondquarter 2015.

[47] F. Pancaldi, G. M. Vitetta, R. Kalbasi, N. Al-Dhahir, M. Uysal, and H. Mheidat, "Single-Carrier Frequency Domain Equalization," *IEEE Signal Processing Magazine*, vol. 25, no. 5, pp. 37–56, September 2008.

[48] R. Rajashekar, K. Hari, and L. Hanzo, "Reduced-Complexity ML Detection and Capacity-Optimized Training for Spatial Modulation Systems," *IEEE Transactions on Communications*, vol. 62, no. 1, pp. 112–125, January 2014.

[49] M. El-Hajjar and L. Hanzo, "EXIT Charts for System Design and Analysis," *IEEE Communications Surveys Tutorials*, vol. 16, no. 1, pp. 127–153, First 2014.

[50] W. Koch and A. Baier, "Optimum And Sub-Optimum Detection of Coded Data Disturbed By Time-Varying Intersymbol Interference," in *Global Telecommunications Conference. 'Communications: Connecting the Future', IEEE*, Dec 1990, pp. 1679–1684 vol.3.

[51] J. Hagenauer, E. Offer, and L. Papke, "Iterative Decoding of Binary Block And Convolutional Codes," *IEEE Transactions on Information Theory*, vol. 42, no. 2, pp. 429–445, Mar 1996.

[52] S. ten Brink, "Convergence of Iterative Decoding," *Electronics Letters*, vol. 35, no. 10, pp. 806–808, May 1999.

[53] A. Ashikhmin, G. Kramer, and S. ten Brink, "Extrinsic Information Transfer Functions: Model And Erasure Channel Properties," *IEEE Transactions on Information Theory*, vol. 50, no. 11, pp. 2657–2673, Nov 2004.

[54] R. Y. S. Tee, R. G. Maunder, and L. Hanzo, "EXIT-chart Aided Near-Capacity Irregular Bit-Interleaved Coded Modulation Design," *IEEE Transactions on Wireless Communications*, vol. 8, no. 1, pp. 32–37, Jan 2009.

[55] I. A. Hemadeh, M. El-Hajjar, S. Won, and L. Hanzo, "Multi-User Steered Multi-Set Space-Time Shift-Keying for Millimeter-Wave Communications," *IEEE Transactions on Vehicular Technology*, vol. PP, no. 99, pp. 1–1, 2016.

[56] I. Hemadeh, M. El-Hajjar, S. Won, and L. Hanzo, "Multi-Set Space-Time Shift Keying And Space-Frequency Space-Time Shift Keying for Millimeter-Wave Communications," *IEEE Access*, vol. PP, no. 99, pp. 1–1, 2016.

[57] M. Kadir, S. Sugiura, J. Zhang, S. Chen, and L. Hanzo, "OFDMA/SC-FDMA Aided Space-Time Shift Keying for Dispersive Multiuser Scenarios," *IEEE Transactions on Vehicular Technology*, vol. 62, no. 1, pp. 408–414, Jan 2013.

[58] M. Kadir, S. Chen, and L. Hanzo, "A Reduced-Complexity Detector for OFDMA/SC-FDMA-Aided Space-Time Shift Keying," in *Vehicular Technology Conference (VTC Fall), IEEE 78th*, Sept 2013, pp. 1–5.

[59] H. Xu, T. Rappaport, R. Boyle, and J. Schaffner, "Measurements And Models for 38-GHz Point-to-Multipoint Radiowave Propagation," *IEEE Journal on Selected Areas in Communications*, vol. 18, no. 3, pp. 310–321, March 2000.

[60] M. Akdeniz, Y. Liu, M. Samimi, S. Sun, S. Rangan, T. Rappaport, and E. Erkip, "Millimeter Wave Channel Modeling and Cellular Capacity Evaluation," *IEEE Journal on Selected Areas in Communications*, vol. 32, no. 6, pp. 1164–1179, June 2014.

[61] S. Chen, A. Livingstone, and L. Hanzo, "Minimum Bit-Error Rate Design For Space-Time Equalization-Based Multiuser Detection," *IEEE Transactions on Communications*, vol. 54, no. 5, pp. 824–832, May 2006.

[62] T. Rappaport, R. Heath, R. Daniels, and J. Murdock, *Millimeter Wave Wireless Communications*, ser. Prentice Hall Communications Engineering and Emerging Technologies Series from Ted Rappaport. Pearson Education, 2014. [Online]. Available: https://books.google.co.uk/books?id=0Jh6BAAAQBAJ

[63] S. Alamouti, "A Simple Transmit Diversity Technique for Wireless Communications," *IEEE Journal on Selected Areas in Communications*, vol. 16, no. 8, pp. 1451–1458, Oct 1998.

[64] P. Wolniansky, G. Foschini, G. Golden, and R. Valenzuela, "V-BLAST: An Architecture for Realizing Very High Data Rates Over The Rich-Scattering Wireless Channel," in *International Symposium on Signals, Systems, and Electronics (ISSSE)*, Sep 1998, pp. 295–300.

[65] B. Hassibi and B. Hochwald, "Linear Dispersion Codes," in *IEEE International Symposium on Information Theory, 2001. Proceedings*, 2001, p. 325.

[66] J. Jeganathan, A. Ghrayeb, and L. Szczecinski, "Spatial Modulation: Optimal Detection And Performance Analysis," *IEEE Communications Letters*, vol. 12, no. 8, pp. 545–547, Aug 2008.

[67] J. Jeganathan, A. Ghrayeb, L. Szczecinski, and A. Ceron, "Space Shift Keying Modulation for MIMO Channels," *IEEE Transactions on Wireless Communications*, vol. 8, no. 7, pp. 3692–3703, July 2009.

Panagiotis Botsinis (S'12-M'15) received the M.Eng. degree from the School of Electrical and Computer Engineering of the National Technical University of Athens (NTUA), Greece, in 2010, as well as the M.Sc. degree with distinction and the Ph.D. degree in Wireless Communications from the University of Southampton, UK, in 2011 and 2015, respectively. He is currently working as a Research Fellow in the Southampton Wireless group at the School of Electronics and Computer Science of the University of Southampton, UK. Since October 2010, he has been a member of the Technical Chamber of Greece. His research interests include quantum-assisted communications, quantum computation, iterative detection, OFDM, MIMO, multiple access systems, coded modulation, channel coding, cooperative communications, as well as combinatorial optimization.

Mohammed El-Hajjar is an Associate Professor in the department of Electronics and Computer Science in the University of Southampton. He received his PhD in Wireless Communications from the University of Southampton, UK in 2008. Following the PhD, he joined Imagination Technologies as a design engineer, where he worked on designing and developing Imagination's multi-standard communications platform, which resulted in three patents. He is the recipient of several academic awards and has published a Wiley-IEEE book and in excess of 80 journal and conference papers. Mohammed's research interests include the development of intelligent communications systems, energy-efficient transceiver design, MIMO, millimeter-wave communications and Radio over fiber network design.

Ibrahim Hemadeh received his BEng degree (with first class honour) in Computer and Communications Engineering from the Islamic University of Lebanon in 2010. He then received an MSc in Wireless Communications (with distinction) from the University of Southampton, UK in 2012. He is currently pursuing his PhD in Wireless Communications with the Univesrity of Southampton under the supervision of Prof Lajos Hanzo and Dr Mohammed El-Hajjar. His research interests mainly include millimeter wave communications, Multi-functional MIMO and Multi-user MIMO.

SeungHwan Won (M'04-SM'16) received the B.S. and M.S. degrees in radio science and engineering from Korea University, Seoul, Republic of Korea, in 1999 and 2001, respectively, and the Ph.D. degree from the Communications Research Group, School of Electronics and Computer Science, University of Southampton, United Kingdom, in 2008. He had been a research engineer with the Mobile Communication Technology Research Laboratory, LG Electronics R&D until September 2004. He was the recipient of the 2004 State Scholarship of the Information and Telecommunication National Scholarship Program, Ministry of Information and Communication, Republic of Korea. After his graduation from University of Southampton, he has been a senior engineer with Modem Team, Digital Media & Communications Business, Samsung Electronics Co. LTD until March 2013. His major research interests encompass synchronisation and detection schemes in diverse MIMO- aided single- and multicarrier systems as well as in MIMO-aided millimetre-wave mobile broadband communication systems with the aid of machine learning. He published a host of papers in these research fields. He is currently with University of Southampton Malaysia Campus in Johor, Malaysia as Associate Professor.

Lajos Hanzo received his degree in electronics in 1976 and his doctorate in 1983. In 2009 he was awarded the honorary doctorate "Doctor Honoris Causa" by the Technical University of Budapest. During his 40-year career in telecommunications he has held various research and academic posts in Hungary, Germany and the UK. Since 1986 he has been with the School of Electronics and Computer Science, University of Southampton, UK, where he holds the chair in telecommunications. He has successfully supervised about 110+ PhD students, co-authored 20 John Wiley/IEEE Press books on mobile radio communications totalling in excess of 10,000 pages, published 1,600+ research entries at IEEE Xplore, acted both as TPC and General Chair of IEEE conferences, presented keynote lectures and has been awarded a number of distinctions. Currently he is directing a 60-strong academic research team, working on a range of research projects in the field of wireless multimedia communications sponsored by industry, the Engineering and Physical Sciences Research Council (EPSRC) UK, the European Research Council's Advanced Fellow Grant and the Royal Society's Wolfson Research Merit Award. He is an enthusiastic supporter of industrial and academic liaison and he offers a range of industrial courses.